Model-independent sensibility studies for the anomalous dipole moments of the ν_τ at the CLIC based e^+e^- and γe^- colliders

A. A. Billur,[1,*] M. Köksal,[2,†] A. Gutiérrez-Rodríguez,[3,‡] and M. A. Hernández-Ruíz[4,§]

[1]Department of Physics, Cumhuriyet University, 58140, Sivas, Turkey
[2]Department of Optical Engineering, Cumhuriyet University, 58140, Sivas, Turkey
[3]Facultad de Física, Universidad Autónoma de Zacatecas, Apartado Postal C-580, 98060 Zacatecas, México
[4]Unidad Académica de Ciencias Químicas, Universidad Autónoma de Zacatecas, Apartado Postal C-585, 98060 Zacatecas, México

(Received 15 September 2018; revised manuscript received 26 September 2018; published 16 November 2018)

To improve the theoretical prediction of the anomalous dipole moments of the τ-neutrino, we have carried out a study through the processes $e^+e^- \to (\gamma, Z) \to \nu_\tau \bar{\nu}_\tau \gamma$ and $\gamma e^- \to \tau \bar{\nu}_\tau \nu_e$, which represent an excellent and useful option in determination of these anomalous parameters. Furthermore, we consider the effective Lagrangian formalism which induces contributions to the dipole moments of the tau-neutrino. To study the potential of the processes $e^+e^- \to (\gamma, Z) \to \nu_\tau \bar{\nu}_\tau \gamma$ and $\gamma e^- \to \tau \bar{\nu}_\tau \nu_e$ we apply a future high-energy and high-luminosity linear electron-positron collider, such as the CLIC, with $\sqrt{s} = 380$, 1500, 3000 GeV and $\mathcal{L} = 10$, 50, 100, 200, 500, 1000, 1500, 2000, 3000 fb^{-1}, and we consider systematic uncertainties of $\delta_{\rm sys} = 0\%$, 5%, 10%. Furthermore, we including initial state radiation plus beamstrahlung effects. With these elements, we present a comprehensive and detailed sensitivity study on the total cross section of the processes $e^+e^- \to (\gamma, Z) \to \nu_\tau \bar{\nu}_\tau \gamma$ and $\gamma e^- \to \tau \bar{\nu}_\tau \nu_e$, as well as on the dipole moments $\tilde{\kappa}_{\nu_\tau}$ and $\tilde{d}_{\nu_\tau}$ at the 95% C.L., showing the feasibility of such processes at the CLIC at the e^+e^- and γe^- modes with unpolarized and polarized electron-positron beams.

DOI: 10.1103/PhysRevD.98.095013

I. INTRODUCTION

The magnetic and electric dipole moments of the neutrino (νMM) and (νEDM) are one of the most sensitive probes of physics beyond the Standard Model (BSM). On this topic, in the original formulation of the Standard Model (SM) [1–3] neutrinos are massless particles with zero νMM. However, in the minimally extended SM containing gauge-singlet right-handed neutrinos, the νMM induced by radiative corrections is unobservably small, $\mu_\nu = 3eG_F m_{\nu_i}/(8\sqrt{2}\pi^2) \simeq 3.1 \times 10^{-19}(m_{\nu_i}/1\,\text{eV})\mu_B$, where $\mu_B = e/2m_e$ is the Bohr magneton [4,5]. Present experimental limits on these νMM are several orders of magnitude larger, so that a MM close to these limits would indicate a window for probing effects induced by new physics BSM [6]. Similarly, a νEDM will also point to new physics and will be of relevance in astrophysics and cosmology, as well as terrestrial neutrino experiments [7].

A fundamental challenge of the particle physics community is to determine the Majorana or Dirac nature of the neutrino. Responding to this challenge, experimentalists are exploring different reactions where the Majorana nature may manifest [8]. About this topic, the study of neutrino magnetic moments is, in principle, a way to distinguish between Dirac and Majorana neutrinos since the Majorana neutrinos can only have flavor changing, transition magnetic moments while the Dirac neutrinos can only have flavor conserving one.

Another fundamental challenge posed by the scientific community is the following: are the laws of physics the same for matter and antimatter, or are matter and antimatter intrinsically different? It is possible that the answer to this problem may hold the key to solving the mystery of the matter-dominated Universe. Sakharov proposed a solution to this problem [9], and this proposal requires the violation of a fundamental symmetry of nature: the CP symmetry. The study of CP violation addresses this problem, as well as many other predicted for the SM. The SM predict CP violation, which is necessary for the existence of the electric dipole moments (EDM) of a variety physical

*abillur@cumhuriyet.edu.tr
†mkoksal@cumhuriyet.edu.tr
‡alexgu@fisica.uaz.edu.mx
§mahernan@uaz.edu.mx

systems. The EDM provides a direct experimental probe of CP violation [10–12], a feature of the SM and beyond SM physics. The signs of new physics can be analyzed by investigating the electromagnetic dipole moments of the tau-neutrino, such as its MM and EDM. In recent years, the ν_τEDM received much attention because the experimental sensitivity is expected to improve considerably in the future. Precise measurement of the ν_τEDM is an important probe of CP violation.

In the case of the ν_eMM and ν_μMM, the best current sensitivity limits are derived from reactor neutrino experiment GEMMA [13] and of the liquid scintillator neutrino detector (LSND) experiment [14], respectively. The obtained sensitivity limits are [13,14]

$$\mu_{\nu_e}^{\rm exp} = 2.9 \times 10^{-11}\mu_B, \qquad 90\%\ \text{C.L.} \quad [\text{GEMMA}], \tag{1}$$

$$\mu_{\nu_\mu}^{\rm exp} = 6.8 \times 10^{-10}\mu_B, \quad 90\%\ \text{C.L.} \quad [\text{LSND}], \tag{2}$$

these limits are 8–9 orders of magnitude weaker than the SM prediction.

For the electric dipole moments d_{ν_e,ν_μ} [15] the best bounds are

$$d_{\nu_e,\nu_\mu} < 2 \times 10^{-21}(e\ \text{cm}), \qquad 95\%\ \text{C.L.} \tag{3}$$

For the tau-neutrino, the bounds on their dipole moments are less restrictive, and therefore it is worth investigating in a deeper way their electromagnetic properties. The τ-neutrino corresponds to the more massive third generation of leptons and possibly possesses the largest mass and the largest magnetic and electric dipole moments.

Table I of Ref. [16] summarizes the current experimental and theoretical bounds on the anomalous dipole moments of the tau-neutrino. The present experimental bounds on the ν_τMM have been reported by different experiments at Borexino [17], E872 (DONUT) [18], CERN-WA-066 [19], and at LEP [20]. In addition, other limits on the ν_τMM and ν_τEDM in different contexts are reported in Refs. [21–42].

A central goal of the physics program of the future lepton colliders is to complement the Large Hadron Collider (LHC) results and also search for clues in BSM. The lepton colliders are designed to study the properties of the new particles and the interactions they might undergo according to the vast amount of theories. Furthermore, the lepton colliders compared to the LHC have a cleaner background, and it is possible to extract the new physics signals from the background more easily. In this regard, there is currently an ongoing effort for the project named the Compact Linear Collider (CLIC) [43–45]. When it is constructed and enters into operation, the e^+e^-, γe^- and $\gamma\gamma$ collision modes will be studied. The CLIC will be a multi-TeV collider and will be operated in three energy stages, corresponding to center-of-mass energies $\sqrt{s} = 380$, 1500, 3000 GeV, and it is an ideal machine to study new physics BSM.

Motivated by the extensive physical program of the CLIC, we conduce a comprehensive study to probe the sensitivity of the processes $e^+e^- \to (\gamma, Z) \to \nu_\tau\bar{\nu}_\tau\gamma$ and $\gamma e^- \to \tau\bar{\nu}_\tau\nu_e$ to the total cross section, the MM and the EDM of the tau-neutrino in a model-independent way. For the study, the beam polarization facility at the CLIC along with the typical center-of-mass energies $\sqrt{s} = 380$, 1500, 3000 GeV and integrated luminosities $\mathcal{L} = 10$, 50, 100, 300, 500, 1000, 1500, 2000, 3000 fb^{-1} are considered. In addition, we estimate the sensitivity at the 95% C.L. and systematic uncertainties $\delta_{\rm sys} = 0\%$, 5%, 10% on the dipole moments of the τ-neutrino. It is shown that the processes under consideration $e^+e^- \to (\gamma, Z) \to \nu_\tau\bar{\nu}_\tau\gamma$ and $\gamma e^- \to \tau\bar{\nu}_\tau\nu_e$ are a good prospect for studying the dipole moments of the tau-neutrino at the CLIC. Furthermore, our study illustrates the complementarity between CLIC and other e^+e^- and pp colliders in probing extensions of the SM, and shows that the CLIC at high energy and high luminosity provides a powerful means to sensitivity estimates for the electromagnetic dipole moments of the tau-neutrino.

This article is organized as follows. In Sec. II, we study the total cross section and the dipole moments of the tau-neutrino through the processes $e^+e^- \to (\gamma, Z) \to \nu_\tau\bar{\nu}_\tau\gamma$ and $\gamma e^- \to \tau\bar{\nu}_\tau\nu_e$ with unpolarized and polarized beams. Section III is devoted to our conclusions.

II. THE TOTAL CROSS SECTION OF THE PROCESSES $e^+e^- \to \nu_\tau\bar{\nu}_\tau\gamma$ AND $\gamma e^- \to \tau\bar{\nu}_\tau\nu_e$ AND DIPOLE MOMENTS

A. Electromagnetic vertex $\nu_\tau\bar{\nu}_\tau\gamma$

Theoretically the electromagnetic properties of neutrinos best studied and well understood are the MM and the EDM. Despite that the neutrino is a neutral particle, neutrinos can interact with a photon through loop (radiative) diagrams. However, a convenient way of studying its electromagnetic properties on a model-independent way is through the effective neutrino-photon interaction vertex which is described by four independent form factors. The most general expression for the vertex of interaction $\nu_\tau\bar{\nu}_\tau\gamma$ is given in Refs. [46–48]. For the study of the MM and the EDM of the tau-neutrino, we are following a focusing as that performed in our previous works [16,21–25,27,28,30–32,35,36] with

$$\begin{aligned}\Gamma^\alpha = {} & eF_1(q^2)\gamma^\alpha + \frac{ie}{2m_{\nu_\tau}}F_2(q^2)\sigma^{\alpha\mu}q_\mu \\ & + \frac{e}{2m_{\nu_\tau}}F_3(q^2)\gamma_5\sigma^{\alpha\mu}q_\mu \\ & + eF_4(q^2)\gamma_5\left(\gamma^\alpha - \frac{\not{q}q^\alpha}{q^2}\right),\end{aligned} \tag{4}$$

where e is the electric charge of the electron, m_{ν_τ} is the mass of the tau-neutrino, q^μ is the photon momentum, and $F_{1,2,3,4}(q^2)$ are the four electromagnetic form factors of the neutrino. In general the $F_{1,2,3,4}(q^2)$ are independent form factors, and they are not physical quantities, but in the limit $q^2 \to 0$ they are quantifiable and related to the static quantities corresponding to charge radius, MM, EDM and anapole moment (AM) of the Dirac neutrinos, respectively [38,49–54]. In this paper we study the anomalous MM ($\mu_{\nu_\tau} = \kappa_{\nu_\tau}\mu_B$) and the EDM ($d_{\nu_\tau}$) of the tau-neutrino, which are defined in terms of the $F_2(q^2=0)$ and $F_3(q^2=0)$ independent form factor as follows:

$$\kappa_{\nu_\tau} = \left(\frac{m_e}{m_{\nu_\tau}}\right) F_2(0), \tag{5}$$

$$d_{\nu_\tau} = \left(\frac{e}{2m_{\nu_\tau}}\right) F_3(0), \tag{6}$$

as we mentioned above. The form factors corresponding to charge radius and the anapole moment are not considered in this paper.

B. The effective Lagrangian and gauge-invariant operators of dimension six

The effective Lagrangian formalism has been utilized extensively for parametrizing new physics BSM in many processes of particle physics. This technique provides a model-independent parametrization of any new physics characterized by higher dimension operators.

The vertex of electromagnetic interaction $\nu_\tau\bar{\nu}_\tau\gamma$ given by Eq. (4) is parametrized in terms of four form factors, with Lorentz invariance and electromagnetic gauge invariance. However, this vertex does not represent the gauge-invariant interaction with respect to the SM gauge group. In this regard, we present gauge-invariant operators of dimension six leading to electromagnetic vertex (4).

The corresponding effective Lagrangian to parametrize deviations from the SM for the anomalous $\nu\bar{\nu}\gamma$ coupling is written in the following form:

$$\mathcal{L}_{\text{eff}} = \mathcal{L}_{\text{SM}} + \sum_n \frac{\alpha_i}{\Lambda^2}\mathcal{O}_n, \tag{7}$$

where $\mathcal{L}_{\text{eff}}$ is the effective Lagrangian which contains operators of increasing dimension that are built with the SM fields, $\mathcal{L}_{\text{SM}}$ is the renormalizable SM Lagrangian, the coefficients α_i depend on the fundamental physics, Λ is the new physics scale and $\mathcal{O}_n$ represents the operator basis composed of the SM fields content, that is to say gauge bosons, Higgs doublets, and fermionic fields. Thus the relevant operators involving the anomalous vertices $\nu\bar{\nu}\gamma$ which arise from the dimension six effective operators [55–57] are

$$\mathcal{O}_{\nu_l B} = \bar{L}\sigma^{\mu\nu}\nu_{lR}\tilde{\Phi}B_{\mu\nu}, \tag{8}$$

$$\mathcal{O}_{\nu_l W} = \bar{L}\sigma^{\mu\nu}\sigma\nu_{lR}\tilde{\Phi}\mathbf{W}_{\mu\nu}, \tag{9}$$

and

$$\tilde{\mathcal{O}}_{\nu_l B} = \bar{L}\sigma^{\mu\nu}i\gamma_5\nu_{lR}\tilde{\Phi}B_{\mu\nu}, \tag{10}$$

$$\tilde{\mathcal{O}}_{\nu_l W} = \bar{L}\sigma^{\mu\nu}i\gamma_5\sigma\nu_{lR}\tilde{\Phi}\mathbf{W}_{\mu\nu}, \tag{11}$$

for the ν_τMM and ν_τEDM, respectively. These operators preserve the $SU(2)_L \times U(1)_Y$ gauge symmetry of the SM. In Eqs. (8)–(11), $\tilde{\Phi}$ and L are the Higgs and the left-handed $SU(2)_L$ doublets which contain ν_l, σ is the Pauli matrices, and $B_{\mu\nu}$ and $\mathbf{W}_{\mu\nu}$ are the $U(1)_Y$ and $SU(2)_L$ gauge field strength tensors.

The effective Lagrangian for examined deviations of the τ-neutrino dipole moments from the SM values is given by

$$\mathcal{L}_{\text{eff}} = \sum_f \left(\frac{\alpha_{fB}}{\Lambda^2}\mathcal{O}_B + \frac{\alpha_W}{\Lambda^2}\mathcal{O}_W\right) + \sum_f \left(\frac{\tilde{\alpha}_{fB}}{\Lambda^2}\tilde{\mathcal{O}}_{fB} + \frac{\tilde{\alpha}_{fW}}{\Lambda^2}\tilde{\mathcal{O}}_{fW}\right). \tag{12}$$

After the spontaneous electroweak symmetry breaking the effective Lagrangian given in Eq. (12) induces contributions to the anomalous magnetic moment κ_{ν_τ} and the electric dipole moment d_{ν_τ} of the tau-neutrino as follows:

$$\tilde{\kappa}_{\nu_\tau} = \frac{2\sqrt{2}m_{\nu_\tau}}{ve}(\cos\theta_W\epsilon_{\nu B} + \sin\theta_W\epsilon_{\nu W}), \tag{13}$$

$$\tilde{d}_{\nu_\tau} = -\frac{\sqrt{2}}{v}(\cos\theta_W\tilde{\epsilon}_{\nu B} + \sin\theta_W\tilde{\epsilon}_{\nu W}), \tag{14}$$

where

$$\epsilon_{\nu B} = \alpha_{\nu B}\frac{v^2}{\Lambda^2}, \tag{15}$$

$$\epsilon_{\nu W} = \alpha_{\nu W}\frac{v^2}{\Lambda^2}, \tag{16}$$

$$\tilde{\epsilon}_{\nu B} = \tilde{\alpha}_{\nu B}\frac{v^2}{\Lambda^2}, \tag{17}$$

$$\tilde{\epsilon}_{\nu W} = \tilde{\alpha}_{\nu W}\frac{v^2}{\Lambda^2}, \tag{18}$$

with $v^2 \simeq (246\ \text{GeV})^2$ and θ_W is the weak mixing angle.

C. The total cross section of the process $e^+e^- \to \nu_\tau\bar{\nu}_\tau\gamma$ beyond the SM with unpolarized electron-positron beams at the CLIC

The CLIC physics program [43–45] is very broad and rich which complements the physics program of the LHC. Furthermore, it provides a unique opportunity to study e^+e^-, $\gamma\gamma$ and γe^- interactions with high energy and high luminosity.

The corresponding Feynman diagrams for the signal $e^+e^- \to (\gamma, Z) \to \nu_\tau\bar{\nu}_\tau\gamma$ are given in Fig. 1. The total cross section of the process $e^+e^- \to \nu_\tau\bar{\nu}_\tau\gamma$ with unpolarized electron-positron beams is computed using the CalcHEP 3.6.30 [58] package, which can compute the Feynman diagrams, integrating over multiparticle phase space and event simulation. Furthermore, in order to select the events we implement the standard isolation cuts, compatibly with the detector resolution expected at CLIC:

$$\begin{aligned} &\text{Cut-1}: \; p_T^\nu > 150 \text{ GeV}, \\ &\text{Cut-2}: \; |\eta^\gamma| < 2.37, \\ &\text{Cut-3}: \; p_T^\gamma > 150 \text{ GeV}, \end{aligned} \tag{19}$$

we apply these cuts to reduce the background and to optimize the signal sensitivity. In Eq. (19), p_T^ν is the transverse momentum of the final state neutrinos, η^γ is the pseudorapidity and p_T^γ is the transverse momentum of the photon. The outgoing particles are required to satisfy these isolation cuts.

Formally, the $e^+e^- \to (\gamma, Z) \to \nu_\tau\bar{\nu}_\tau\gamma$ cross section can be split into two parts:

$$\sigma = \sigma_{\text{BSM}} + \sigma_0, \tag{20}$$

where σ_{BSM} is the contribution due to BSM physics, which, in our case comes from the anomalous vertex $\nu_\tau\bar{\nu}_\tau\gamma$, while

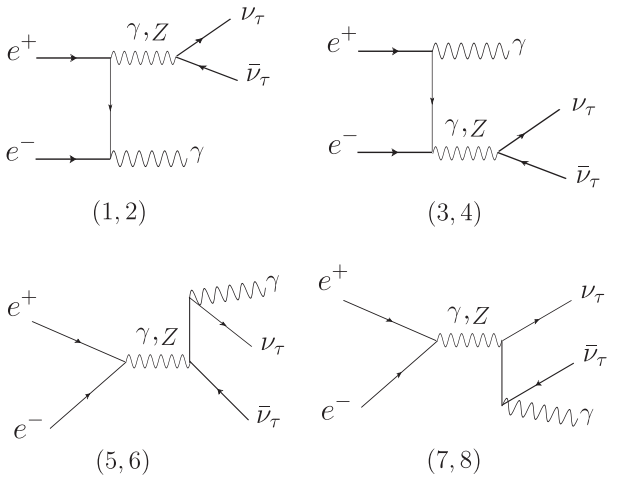

FIG. 1. The Feynman diagrams for the process $e^+e^- \to (\gamma, Z) \to \nu_\tau\bar{\nu}_\tau\gamma$.

σ_0 is the SM prediction. The analytical expression for the squared amplitudes is quite lengthy so we do not present it here. Following the form of Eq. (20), we present numerical fit functions for the total cross section with respect to center-of-mass energy, with unpolarized electron-positron beams and in terms of the independent factors $\tilde{\kappa}_{\nu_\tau}(\tilde{d}_{\nu_\tau})$.

(i) For $\sqrt{s} = 380$ GeV:

$$\begin{aligned} \sigma(\tilde{\kappa}_{\nu_\tau}) &= [(2.68 \times 10^{11})\tilde{\kappa}_{\nu_\tau}^4 + (1.97 \times 10^4)\tilde{\kappa}_{\nu_\tau}^2 \\ &\quad + 0.041](\text{pb}), \\ \sigma(\tilde{d}_{\nu_\tau}) &= [(2.68 \times 10^{11})\tilde{d}_{\nu_\tau}^4 + (1.97 \times 10^4)\tilde{d}_{\nu_\tau}^2 \\ &\quad + 0.041](\text{pb}). \end{aligned} \tag{21}$$

(ii) For $\sqrt{s} = 1.5$ TeV:

$$\begin{aligned} \sigma(\tilde{\kappa}_{\nu_\tau}) &= [(3.32 \times 10^{13})\tilde{\kappa}_{\nu_\tau}^4 + (5.13 \times 10^5)\tilde{\kappa}_{\nu_\tau}^2 \\ &\quad + 0.012](\text{pb}), \\ \sigma(\tilde{d}_{\nu_\tau}) &= [(3.32 \times 10^{13})\tilde{d}_{\nu_\tau}^4 + (5.13 \times 10^5)\tilde{d}_{\nu_\tau}^2 \\ &\quad + 0.012](\text{pb}). \end{aligned} \tag{22}$$

(iii) For $\sqrt{s} = 3$ TeV:

$$\begin{aligned} \sigma(\tilde{\kappa}_{\nu_\tau}) &= [(1.49 \times 10^{14})\tilde{\kappa}_{\nu_\tau}^4 + (9.70 \times 10^5)\tilde{\kappa}_{\nu_\tau}^2 \\ &\quad + 0.003](\text{pb}), \\ \sigma(\tilde{d}_{\nu_\tau}) &= [(1.49 \times 10^{14})\tilde{d}_{\nu_\tau}^4 + (9.70 \times 10^5)\tilde{d}_{\nu_\tau}^2 \\ &\quad + 0.003](\text{pb}). \end{aligned} \tag{23}$$

It is worth mentioning that in Eqs. (21)–(23), the coefficients of $\tilde{\kappa}_{\nu_\tau}(\tilde{d}_{\nu_\tau})$ give the anomalous contribution, while the independent terms of $\tilde{\kappa}_{\nu_\tau}(\tilde{d}_{\nu_\tau})$ correspond to the cross section at $\tilde{\kappa}_{\nu_\tau} = \tilde{d}_{\nu_\tau} = 0$ and represent the SM total cross-section magnitude.

D. Sensitivity estimates on the $\tilde{\kappa}_{\nu_\tau}$ and $\tilde{d}_{\nu_\tau}$ with unpolarized electron-positron beams

Based on the formulas given by Eqs. (21)–(23), we make model-independent sensitivity estimates for the total cross section of the signal $\sigma(e^+e^- \to \nu_\tau\bar{\nu}_\tau\gamma) = \sigma(\sqrt{s}, \tilde{\kappa}_{\nu_\tau}, \tilde{d}_{\nu_\tau})$, as well as for the $\tilde{\kappa}_{\nu_\tau}$ and $\tilde{d}_{\nu_\tau}$ at the CLIC. To carry out this task, we consider the acceptance cuts given in Eq. (19) and we take into account the systematic uncertainties $\delta_{\text{sys}} = 0\%$, 5%, 10% for the collider. In addition to sensitivity estimates on the parameters of the process $e^+e^- \to \nu_\tau\bar{\nu}_\tau\gamma$, we use the χ^2 function [16,42,59–64]

$$\chi^2 = \left(\frac{\sigma_{\text{SM}} - \sigma(\sqrt{s}, \tilde{\kappa}_{\nu_\tau}, \tilde{d}_{\nu_\tau})}{\sigma_{\text{SM}} \sqrt{(\delta_{st})^2 + (\delta_{\text{sys}})^2}} \right)^2, \tag{24}$$

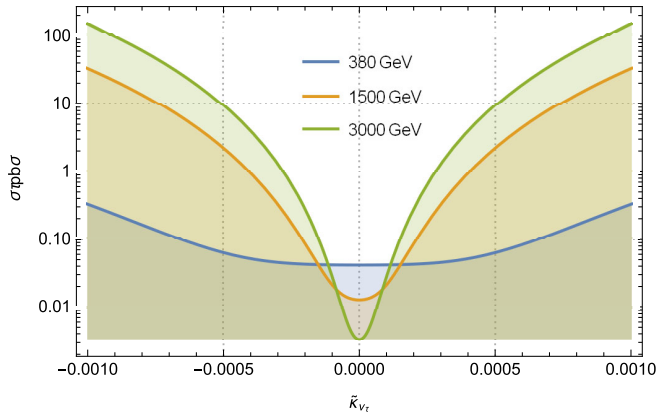

FIG. 2. The total cross sections of the process $e^+e^- \to \nu_\tau\bar{\nu}_\tau\gamma$ as a function of $\tilde{\kappa}_{\nu_\tau}$ for center-of-mass energies of $\sqrt{s} = 380$, 1500, 3000 GeV.

where $\sigma(\sqrt{s}, \tilde{\kappa}_{\nu_\tau}, \tilde{d}_{\nu_\tau})$ is the total cross section including contributions from the SM and new physics, $\delta_{st} = \frac{1}{\sqrt{N_{\rm SM}}}$ is the statistical error and $\delta_{\rm sys}$ is the systematic error. The number of events is given by $N_{\rm SM} = \mathcal{L}_{\rm int} \times \sigma_{\rm SM}$, where $\mathcal{L}_{\rm int}$ is the integrated CLIC luminosity.

As stated in the Introduction, to carry out our study we considered the typical center-of-mass energies $\sqrt{s} = 380$, 1500, 3000 GeV and integrated luminosities $\mathcal{L} = 10$, 50, 100, 300, 500, 1000, 1500, 2000, 3000 fb^{-1} of the CLIC.

We report in Figs. 2 and 3 the sensitivity on the signal cross section $e^+e^- \to (\gamma, Z) \to \nu_\tau\bar{\nu}_\tau\gamma$ at the CLIC as a function of the factors $\tilde{\kappa}_{\nu_\tau}(\tilde{d}_{\nu_\tau})$ and for different center-of-mass energies $\sqrt{s} = 380$, 1500, 3000 GeV. Clearly the total cross section is dominant for $\sqrt{s} = 3000$ GeV and for large values of the factors $\tilde{\kappa}_{\nu_\tau}(\tilde{d}_{\nu_\tau})$, and decreases as $\tilde{\kappa}_{\nu_\tau}(\tilde{d}_{\nu_\tau})$ tends to zero, recovering the value of the SM as shown in Eq. (23).

Sensitivity contours at the 95% C.L. in the $\tilde{\kappa}_{\nu_\tau} - \tilde{d}_{\nu_\tau}$ plane for the signal $e^+e^- \to \nu_\tau\bar{\nu}_\tau\gamma$ with center-of-mass energies $\sqrt{s} = 380$, 1500, 3000 GeV and luminosities

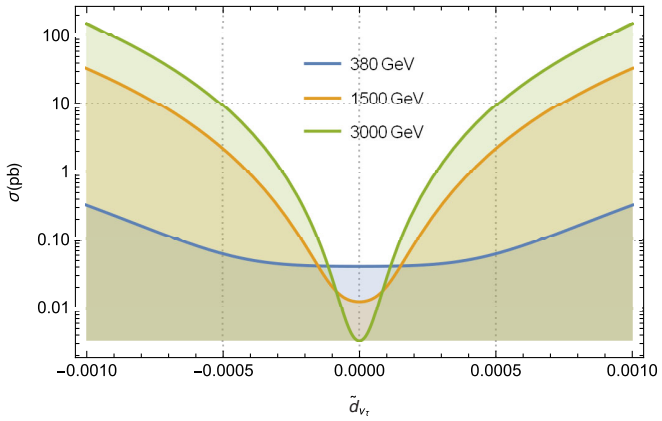

FIG. 3. Same as in Fig. 2, but for $\tilde{d}_{\nu_\tau}$.

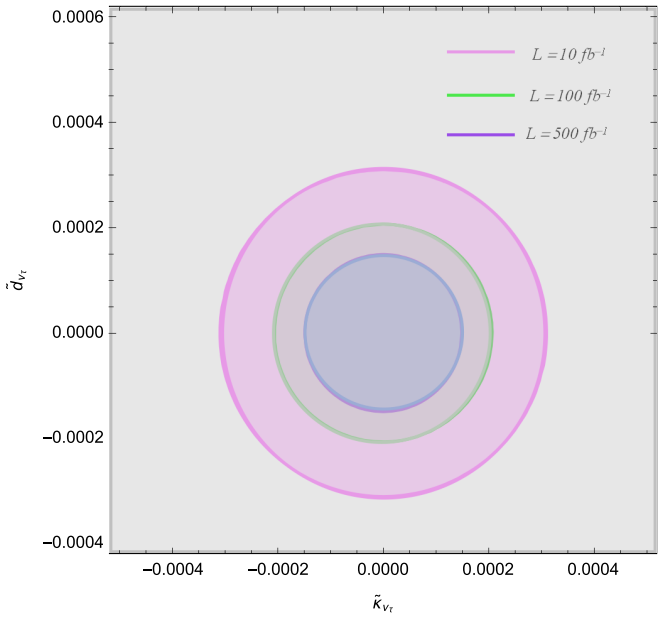

FIG. 4. Sensitivity contours at the 95% C.L. in the $\tilde{\kappa}_{\nu_\tau} - \tilde{d}_{\nu_\tau}$ plane for the process $e^+e^- \to \nu_\tau\bar{\nu}_\tau\gamma$ with the $\delta_{\rm sys} = 0\%$ and for center-of-mass energy of $\sqrt{s} = 380$ GeV.

$\mathcal{L} = 10$, 100, 500, 1500, 3000 fb^{-1} are given in Figs. 4–6. As highlighted in Fig. 6, the three most sensitive contours for $\tilde{\kappa}_{\nu_\tau}$ and $\tilde{d}_{\nu_\tau}$ are the corresponding ones for high energy and high luminosity of $\sqrt{s} = 3000$ GeV and $\mathcal{L} = 3000$ fb^{-1}.

As a final result on our sensitivity analysis, we stress the sensitivity estimates on the $\tilde{\kappa}_{\nu_\tau}$ and $\tilde{d}_{\nu_\tau}$ via the channel $e^+e^- \to \nu_\tau\bar{\nu}_\tau\gamma$ for $\sqrt{s} = 380$, 1500, 3000 GeV, $\mathcal{L} = 10$, 50, 100, 300, 500, 1000, 1500, 2000, 3000 fb^{-1}, $\delta_{\rm sys} = 0\%$, 5%, 10% at 90% C.L. and 95% C.L. We show our results in

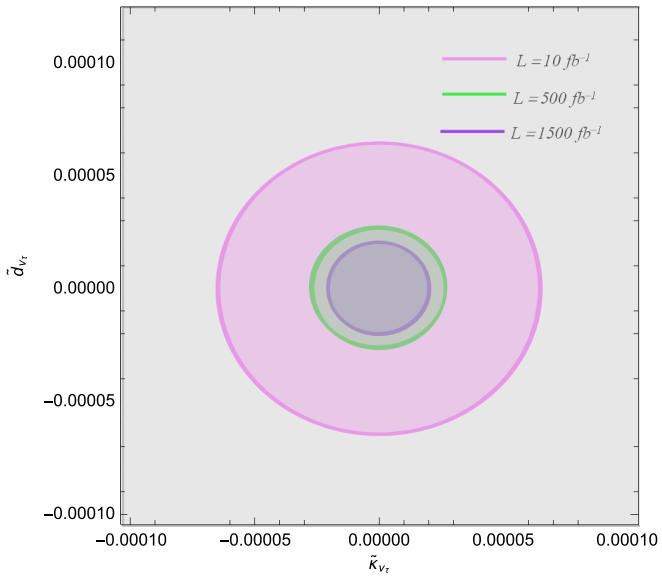

FIG. 5. Same as in Fig. 4, but for $\sqrt{s} = 1500$ GeV.

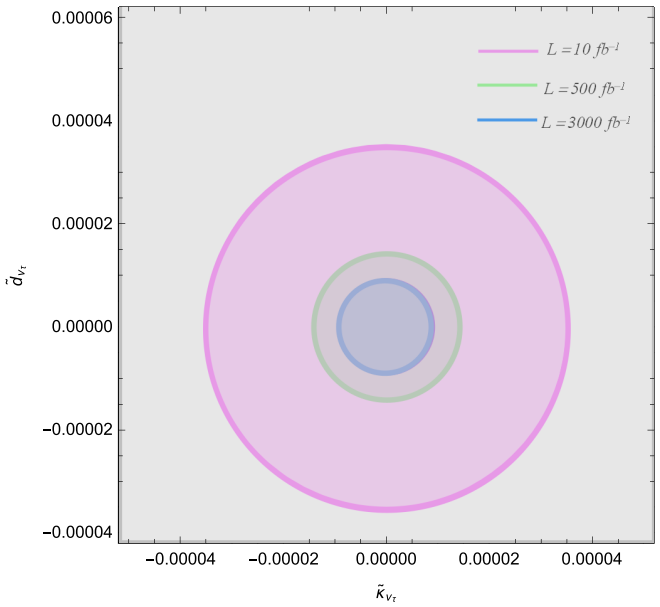

FIG. 6. Same as in Fig. 4, but for $\sqrt{s} = 3000$ GeV.

Tables I–III, where the better sensitivity on the dipole moments of the τ-neutrino projected for the CLIC are for $\sqrt{s} = 3000$ GeV and $\mathcal{L} = 3000$ fb^{-1}: $|\tilde{\kappa}_{\nu_\tau}| = 2.103 \times 10^{-7}$ and $|\tilde{d}_{\nu_\tau}(e\ \text{cm})| = 4.076 \times 10^{-18}$ at 90% C.L.

E. The total cross section of the process $e^+e^- \to \nu_\tau\bar{\nu}_\tau\gamma$ beyond the SM with polarized electron-positron beams at the CLIC

Another option for a sensitivity study of the total production of the channel $e^+e^- \to \nu_\tau\bar{\nu}_\tau\gamma$, in addition to the dipole moments of the tau-neutrino is the electron-positron beams polarization facility at the CLIC. The possibility of using polarized electron and positron beams can constitute a strong advantage in searching for new physics [65]. Furthermore, the electron-positron beam polarization may lead to a reduction of the measurement uncertainties, either by increasing the signal cross section, therefore reducing the statistical uncertainty, or by suppressing important backgrounds. In summary, one other option at the CLIC is to polarize the incoming beams, which could maximize the physics potential, both in the performance of precision tests and in revealing the properties of the new physics BSM.

The general formula for the total cross section for an arbitrary degree of longitudinal e^- and e^+ beams polarization is given by [65]

$$\begin{aligned}\sigma(P_{e^-}, P_{e^+}) = \frac{1}{4}[&(1+P_{e^-})(1+P_{e^+})\sigma_{++} \\ &+ (1-P_{e^-})(1-P_{e^+})\sigma_{--} \\ &+ (1+P_{e^-})(1-P_{e^+})\sigma_{+-} \\ &+ (1-P_{e^-})(1+P_{e^+})\sigma_{-+}], \end{aligned} \tag{25}$$

where $P_{e^-}(P_{e^+})$ is the polarization degree of the electron (positron) beam, while σ_{-+} stands for the cross section for completely left-handed polarized e^- beam $P_{e^-} = -1$ and completely right-handed polarized e^+ beam $P_{e^+} = 1$, and other cross sections σ_{--}, σ_{++} and σ_{+-} are defined analogously.

TABLE I. Sensitivity estimates on the $\tilde{\kappa}_{\nu_\tau}$ magnetic moment and $\tilde{d}_{\nu_\tau}$ electric dipole moment via the process $e^+e^- \to \nu_\tau\bar{\nu}_\tau\gamma$ for $\sqrt{s} = 380$ GeV and $P_{e^-} = P_{e^+} = 0\%$.

90% C.L. $\sqrt{s} = 380$ GeV						
	$\delta_{\text{sys}} = 0\%$		$\delta_{\text{sys}} = 5\%$		$\delta_{\text{sys}} = 10\%$	
$\mathcal{L}$(fb^{-1})	$\lvert\tilde{\kappa}_{\nu_\tau}\rvert$	$\lvert\tilde{d}_{\nu_\tau}(e\ \text{cm})\rvert$	$\lvert\tilde{\kappa}_{\nu_\tau}\rvert$	$\lvert\tilde{d}_{\nu_\tau}(e\ \text{cm})\rvert$	$\lvert\tilde{\kappa}_{\nu_\tau}\rvert$	$\lvert\tilde{d}_{\nu_\tau}(e\ \text{cm})\rvert$
10	7.953×10^{-6}	1.541×10^{-16}	8.914×10^{-6}	1.727×10^{-16}	1.028×10^{-5}	1.993×10^{-16}
50	6.031×10^{-6}	1.168×10^{-16}	8.225×10^{-6}	1.594×10^{-16}	1.002×10^{-5}	1.943×10^{-16}
100	5.308×10^{-6}	1.028×10^{-16}	8.113×10^{-6}	1.572×10^{-16}	9.988×10^{-6}	1.935×10^{-16}
300	4.285×10^{-6}	8.304×10^{-17}	8.032×10^{-6}	1.556×10^{-16}	9.964×10^{-6}	1.930×10^{-16}
500	3.860×10^{-6}	7.481×10^{-17}	8.016×10^{-6}	1.553×10^{-16}	9.959×10^{-6}	1.929×10^{-16}
95% C.L. $\sqrt{s} = 380$ GeV						
	$\delta_{\text{sys}} = 0\%$		$\delta_{\text{sys}} = 5\%$		$\delta_{\text{sys}} = 10\%$	
$\mathcal{L}$(fb^{-1})	$\lvert\tilde{\kappa}_{\nu_\tau}\rvert$	$\lvert\tilde{d}_{\nu_\tau}(e\ \text{cm})\rvert$	$\lvert\tilde{\kappa}_{\nu_\tau}\rvert$	$\lvert\tilde{d}_{\nu_\tau}(e\ \text{cm})\rvert$	$\lvert\tilde{\kappa}_{\nu_\tau}\rvert$	$\lvert\tilde{d}_{\nu_\tau}(e\ \text{cm})\rvert$
10	8.417×10^{-6}	1.631×10^{-16}	9.415×10^{-6}	1.824×10^{-16}	1.084×10^{-5}	2.101×10^{-16}
50	6.418×10^{-6}	1.243×10^{-16}	8.700×10^{-6}	1.685×10^{-16}	1.057×10^{-5}	2.048×10^{-16}
100	5.664×10^{-6}	1.097×10^{-16}	8.583×10^{-6}	1.663×10^{-16}	1.053×10^{-5}	2.040×10^{-16}
300	4.593×10^{-6}	8.901×10^{-17}	8.499×10^{-6}	1.647×10^{-16}	1.051×10^{-5}	2.035×10^{-16}
500	4.147×10^{-6}	8.036×10^{-17}	8.482×10^{-6}	1.643×10^{-16}	1.050×10^{-5}	2.034×10^{-16}

TABLE II. Sensitivity estimates on the $\tilde{\kappa}_{\nu_\tau}$ magnetic moment and $\tilde{d}_{\nu_\tau}$ electric dipole moment via the process $e^+e^- \to \nu_\tau\bar{\nu}_\tau\gamma$ for $\sqrt{s} = 1500$ GeV and $P_{e^-} = P_{e^+} = 0\%$.

90% C.L. $\sqrt{s} = 1500$ GeV						
	$\delta_{\rm sys} = 0\%$		$\delta_{\rm sys} = 5\%$		$\delta_{\rm sys} = 10\%$	
$\mathcal{L}(\text{fb}^{-1})$	$\lvert\tilde{\kappa}_{\nu_\tau}\rvert$	$\lvert\tilde{d}_{\nu_\tau}(e\ \text{cm})\rvert$	$\lvert\tilde{\kappa}_{\nu_\tau}\rvert$	$\lvert\tilde{d}_{\nu_\tau}(e\ \text{cm})\rvert$	$\lvert\tilde{\kappa}_{\nu_\tau}\rvert$	$\lvert\tilde{d}_{\nu_\tau}(e\ \text{cm})\rvert$
10	1.538×10^{-6}	2.980×10^{-17}	1.630×10^{-6}	3.160×10^{-17}	1.826×10^{-6}	3.539×10^{-17}
100	9.145×10^{-7}	1.772×10^{-17}	1.268×10^{-6}	2.458×10^{-17}	1.643×10^{-6}	3.184×10^{-17}
500	6.225×10^{-7}	1.206×10^{-17}	1.209×10^{-6}	2.343×10^{-17}	1.622×10^{-6}	3.143×10^{-17}
1000	5.258×10^{-7}	1.018×10^{-17}	1.201×10^{-6}	2.327×10^{-17}	1.619×10^{-6}	3.138×10^{-17}
1500	4.760×10^{-7}	9.225×10^{-18}	1.198×10^{-6}	2.321×10^{-17}	1.618×10^{-6}	3.136×10^{-17}
95% C.L. $\sqrt{s} = 1500$ GeV						
	$\delta_{\rm sys} = 0\%$		$\delta_{\rm sys} = 5\%$		$\delta_{\rm sys} = 10\%$	
$\mathcal{L}(\text{fb}^{-1})$	$\lvert\tilde{\kappa}_{\nu_\tau}\rvert$	$\lvert\tilde{d}_{\nu_\tau}(e\ \text{cm})\rvert$	$\lvert\tilde{\kappa}_{\nu_\tau}\rvert$	$\lvert\tilde{d}_{\nu_\tau}(e\ \text{cm})\rvert$	$\lvert\tilde{\kappa}_{\nu_\tau}\rvert$	$\lvert\tilde{d}_{\nu_\tau}(e\ \text{cm})\rvert$
10	1.656×10^{-6}	3.210×10^{-17}	1.754×10^{-6}	3.400×10^{-16}	1.960×10^{-6}	3.799×10^{-17}
100	9.921×10^{-7}	1.922×10^{-17}	1.370×10^{-6}	2.656×10^{-17}	1.767×10^{-6}	3.425×10^{-17}
500	6.772×10^{-7}	1.312×10^{-17}	1.307×10^{-6}	2.533×10^{-17}	1.745×10^{-6}	3.382×10^{-17}
1000	5.724×10^{-7}	1.109×10^{-17}	1.298×10^{-6}	2.516×10^{-17}	1.742×10^{-6}	3.377×10^{-17}
1500	5.185×10^{-7}	1.004×10^{-17}	1.295×10^{-6}	2.510×10^{-17}	1.741×10^{-6}	3.375×10^{-17}

TABLE III. Sensitivity estimates on the $\tilde{\kappa}_{\nu_\tau}$ magnetic moment and $\tilde{d}_{\nu_\tau}$ electric dipole moment via the process $e^+e^- \to \nu_\tau\bar{\nu}_\tau\gamma$ for $\sqrt{s} = 3000$ GeV and $P_{e^-} = P_{e^+} = 0\%$.

90% C.L. $\sqrt{s} = 3000$ GeV						
	$\delta_{\rm sys} = 0\%$		$\delta_{\rm sys} = 5\%$		$\delta_{\rm sys} = 10\%$	
$\mathcal{L}(\text{fb}^{-1})$	$\lvert\tilde{\kappa}_{\nu_\tau}\rvert$	$\lvert\tilde{d}_{\nu_\tau}(e\ \text{cm})\rvert$	$\lvert\tilde{\kappa}_{\nu_\tau}\rvert$	$\lvert\tilde{d}_{\nu_\tau}(e\ \text{cm})\rvert$	$\lvert\tilde{\kappa}_{\nu_\tau}\rvert$	$\lvert\tilde{d}_{\nu_\tau}(e\ \text{cm})\rvert$
100	4.834×10^{-7}	9.368×10^{-18}	5.593×10^{-7}	1.083×10^{-17}	6.844×10^{-7}	1.326×10^{-17}
500	3.272×10^{-7}	6.341×10^{-18}	4.885×10^{-7}	1.081×10^{-17}	6.532×10^{-7}	1.265×10^{-17}
1000	2.759×10^{-7}	5.348×10^{-18}	4.769×10^{-7}	9.242×10^{-18}	6.489×10^{-7}	1.257×10^{-17}
2000	2.325×10^{-7}	4.506×10^{-18}	4.707×10^{-7}	9.122×10^{-18}	6.468×10^{-7}	1.253×10^{-17}
3000	2.103×10^{-7}	4.076×10^{-18}	4.686×10^{-7}	9.081×10^{-18}	6.460×10^{-7}	1.251×10^{-17}
95% C.L. $\sqrt{s} = 3000$ GeV						
	$\delta_{\rm sys} = 0\%$		$\delta_{\rm sys} = 5\%$		$\delta_{\rm sys} = 10\%$	
$\mathcal{L}(\text{fb}^{-1})$	$\lvert\tilde{\kappa}_{\nu_\tau}\rvert$	$\lvert\tilde{d}_{\nu_\tau}(e\ \text{cm})\rvert$	$\lvert\tilde{\kappa}_{\nu_\tau}\rvert$	$\lvert\tilde{d}_{\nu_\tau}(e\ \text{cm})\rvert$	$\lvert\tilde{\kappa}_{\nu_\tau}\rvert$	$\lvert\tilde{d}_{\nu_\tau}(e\ \text{cm})\rvert$
100	5.254×10^{-7}	1.018×10^{-17}	6.071×10^{-7}	1.176×10^{-17}	7.414×10^{-7}	1.436×10^{-17}
500	3.563×10^{-7}	6.905×10^{-18}	5.309×10^{-7}	1.028×10^{-17}	7.080×10^{-7}	1.371×10^{-17}
1000	3.007×10^{-7}	5.826×10^{-18}	5.183×10^{-7}	1.004×10^{-17}	7.034×10^{-7}	1.363×10^{-17}
2000	2.534×10^{-7}	4.912×10^{-18}	5.116×10^{-7}	9.915×10^{-18}	7.010×10^{-7}	1.358×10^{-17}
3000	2.293×10^{-7}	4.443×10^{-18}	5.093×10^{-7}	9.870×10^{-18}	7.002×10^{-7}	1.357×10^{-17}

For our sensitivity study, we assume for definiteness an electron-positron beam polarization $(P_{e^-}, P_{e^+}) = (-80\%, 60\%)$ in the estimated range of the expected CLIC operation setup. Besides the polarized beams we consider the isolation cuts given for Eq. (19).

The numerical fit functions for the total cross sections of the process $e^+e^- \to \nu_\tau\bar{\nu}_\tau\gamma$, following the form of Eq. (21) with polarized electron-positron beams, and in terms of the independent factors $\tilde{\kappa}_{\nu_\tau}(\tilde{d}_{\nu_\tau})$ are given by:

(i) For $\sqrt{s} = 380$ GeV:

$$\begin{aligned}\sigma(\tilde{\kappa}_{\nu_\tau}) &= [(3.97 \times 10^{11})\tilde{\kappa}^4_{\nu_\tau} + (3.16 \times 10^4)\tilde{\kappa}^2_{\nu_\tau} \\ &\quad + 0.072](\text{pb}), \\ \sigma(\tilde{d}_{\nu_\tau}) &= [(3.97 \times 10^{11})\tilde{d}^4_{\nu_\tau} + (3.16 \times 10^4)\tilde{d}^2_{\nu_\tau} \\ &\quad + 0.072](\text{pb}). \end{aligned} \tag{26}$$

(ii) For $\sqrt{s} = 1.5$ TeV:

$$\sigma(\tilde{\kappa}_{\nu_\tau}) = [(4.93 \times 10^{13})\tilde{\kappa}^4_{\nu_\tau} + (7.23 \times 10^5)\tilde{\kappa}^2_{\nu_\tau} + 0.023](\text{pb}),$$
$$\sigma(\tilde{d}_{\nu_\tau}) = [(4.93 \times 10^{13})\tilde{d}^4_{\nu_\tau} + (7.23 \times 10^5)\tilde{d}^2_{\nu_\tau} + 0.023](\text{pb}). \quad (27)$$

(iii) For $\sqrt{s} = 3$ TeV:

$$\sigma(\tilde{\kappa}_{\nu_\tau}) = [(2.23 \times 10^{14})\tilde{\kappa}^4_{\nu_\tau} + (1.43 \times 10^6)\tilde{\kappa}^2_{\nu_\tau} + 0.006](\text{pb}),$$
$$\sigma(\tilde{d}_{\nu_\tau}) = [(2.23 \times 10^{14})\tilde{d}^4_{\nu_\tau} + (1.43 \times 10^6)\tilde{d}^2_{\nu_\tau} + 0.006](\text{pb}). \quad (28)$$

In Eqs. (26)–(28), the coefficients of $\tilde{\kappa}_{\nu_\tau}(\tilde{d}_{\nu_\tau})$ give the anomalous contribution, while the independent terms of $\tilde{\kappa}_{\nu_\tau}(\tilde{d}_{\nu_\tau})$ correspond to the cross section at $\tilde{\kappa}_{\nu_\tau} = \tilde{d}_{\nu_\tau} = 0$ and represent the SM cross section.

F. Sensitivity estimates on the $\tilde{\kappa}_{\nu_\tau}$ and $\tilde{d}_{\nu_\tau}$ with polarized electron-positron beams

The $e^+e^- \to \nu_\tau\bar{\nu}_\tau\gamma$ production cross section, as a function of $\tilde{\kappa}_{\nu_\tau}(\tilde{d}_{\nu_\tau})$ projected for the CLIC with polarized electron-positron beams $(P_{e^-}, P_{e^+}) = (-80\%, 60\%)$ and for the center-of-mass energies $\sqrt{s} = 380$, 1500, 3000 GeV, is shown in Figs. 7 and 8. From the direct comparison of Figs. 7 and 8, with the unpolarized case Figs. 2 and 3, a significant gradual increase in the total production cross sections of 0.6, 60 and 100 pb is clearly shown. In addition, the cross section increases with the increase of $\tilde{\kappa}_{\nu_\tau}(\tilde{d}_{\nu_\tau})$, and decreases as $\tilde{\kappa}_{\nu_\tau}(\tilde{d}_{\nu_\tau})$ decreases. The SM result for the production cross section of the reaction $e^+e^- \to \nu_\tau\bar{\nu}_\tau\gamma$ is obtained in the limit when $\tilde{\kappa}_{\nu_\tau}(\tilde{d}_{\nu_\tau}) = 0$. In this case, the terms that depend on $\tilde{\kappa}_{\nu_\tau}(\tilde{d}_{\nu_\tau})$ in Eqs. (26)–(28) are zero and Eqs. (26)–(28) are reduced to the result for the SM.

Taking $(P_{e^-}, P_{e^+}) = (-80\%, 60\%)$, $\sqrt{s} = 380$, 1500, 3000 GeV and $\mathcal{L} = 10$, 100, 500, 1500, 3000 fb^{-1}, the contours for estimating the sensitivity of $\tilde{\kappa}_{\nu_\tau}$ and $\tilde{d}_{\nu_\tau}$ in the $\tilde{\kappa}_{\nu_\tau} - \tilde{d}_{\nu_\tau}$ plane through the reaction $e^+e^- \to \nu_\tau\bar{\nu}_\tau\gamma$ are evaluated and shown in Figs. 9–11. Figure 11 illustrates the better sensitivity for $\tilde{\kappa}_{\nu_\tau}$ and $\tilde{d}_{\nu_\tau}$ with $\sqrt{s} = 3000$ GeV and $\mathcal{L} = 10$, 500, 3000 fb^{-1}.

Our results given in Tables IV–VI give the sensitivity estimates on $\tilde{\kappa}_{\nu_\tau}$ and $\tilde{d}_{\nu_\tau}$ via the process $e^+e^- \to \nu_\tau\bar{\nu}_\tau\gamma$ for $P_{e^-} = -80\%$, $P_{e^+} = 60\%$, $\sqrt{s} = 380$, 1500, 3000 GeV, $\mathcal{L} = 10$, 50, 100, 300, 500, 1000, 1500, 2000, 3000 fb^{-1}, $\delta_{\text{sys}} = 0\%$, 5%, 10% at 90% C.L. and 95% C.L. The effect of the polarized incoming e^- and e^+ beams shows that the

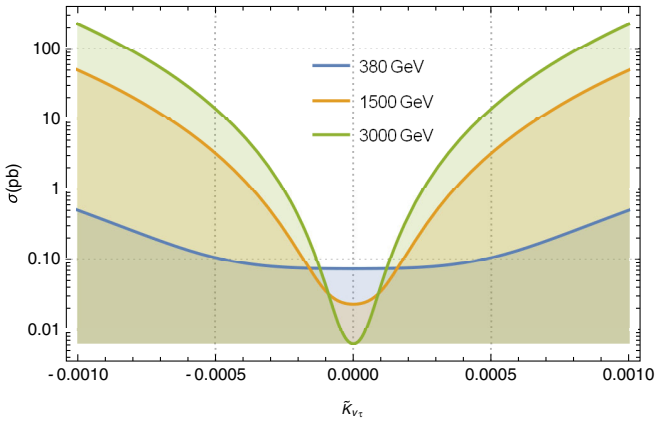

FIG. 7. Same as in Fig. 2, but for $P_{e^-} = -80\%$ and $P_{e^+} = 60\%$.

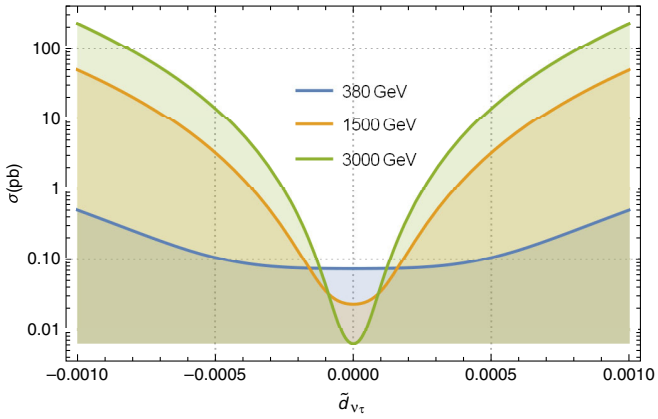

FIG. 8. Same as in Fig. 3, but for $P_{e^-} = -80\%$ and $P_{e^+} = 60\%$.

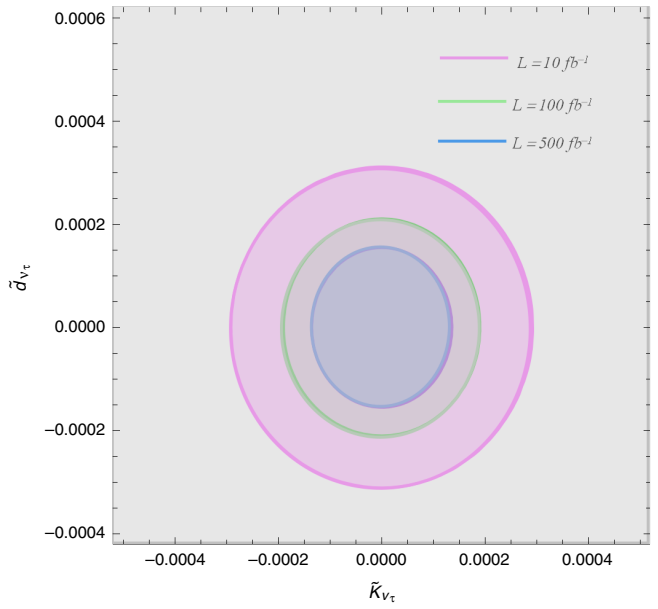

FIG. 9. Same as in Fig. 4, but for $P_{e^-} = -80\%$ and $P_{e^+} = 60\%$.

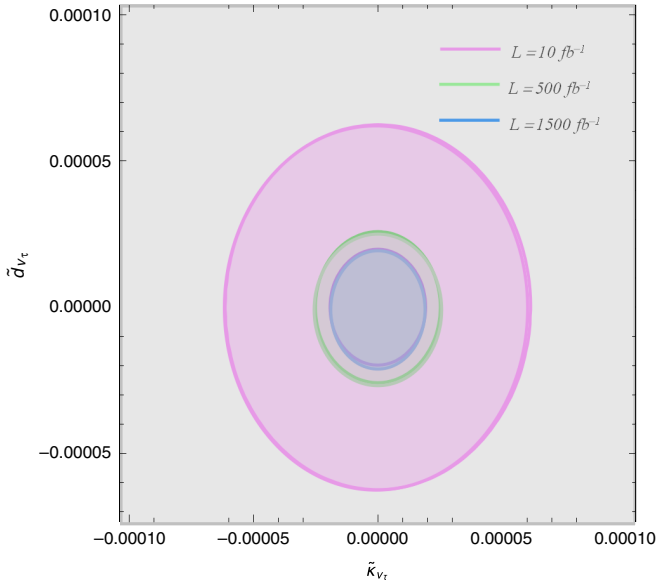

FIG. 10. Same as in Fig. 5, but for $P_{e^-} = -80\%$ and $P_{e^+} = 60\%$.

sensitivity on the $\tilde{\kappa}_{\nu_\tau}$ and $\tilde{d}_{\nu_\tau}$ is enhanced by 5% at $P(-80\%; 60\%)$ polarization configuration, with respect to the unpolarized case (see Tables I–III). Our most relevant results are: $|\tilde{\kappa}_{\nu_\tau}| = 2.002 \times 10^{-7}$ and $|\tilde{d}_{\nu_\tau}(e\ \mathrm{cm})| = 4.039 \times 10^{-18}$ at 90% C.L.

G. Sensitivity estimates on the $\tilde{\kappa}_{\nu_\tau}$ and $\tilde{d}_{\nu_\tau}$ with unpolarized and polarized electron-positron beams, including ISR + BS effects

Electromagnetic radiation emitted by the colliding beams is expected to play an important role at the future high energy e^+e^- linear colliders. Focusing on the processes $e^+e^- \to \nu_\tau \bar{\nu}_\tau \gamma$ and $\gamma e^- \to \tau \bar{\nu}_\tau \nu_e$ (see next subsections), we show that radiative effects like initial state radiation (ISR) and beamstrahlung (BS) can lead to increasing or decreasing the sensitivity of the signal. Thus, precise knowledge of the backgrounds coming from ISR plus BS is essential if we wish to make any realistic predictions at the future linear colliders.

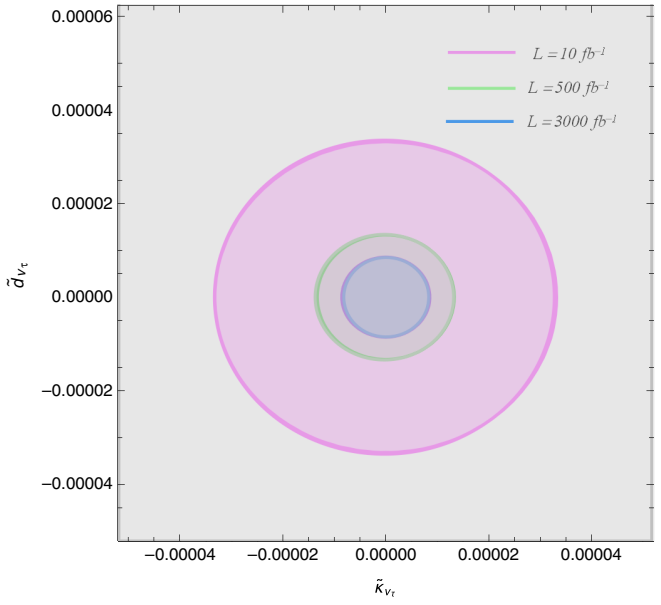

FIG. 11. Same as in Fig. 6, but for $P_{e^-} = -80\%$ and $P_{e^+} = 60\%$.

As we mentioned above, it is essential to consider the ISR and BS in the future linear colliders. ISR is the photon radiation from incoming $e^\pm$ beams and beamstrahlung is the radiation from the incoming beam caused by its interaction with the field of the other beam moving in the opposite direction. In both cases, the initial $e^\pm$ radiates one or more photons which reduce the beam energy and dissipate the beam collimation. Unlike the ISR spectrum, the beamstrahlung spectrum depends not only on the electron beam energy E_e, but also on the highly machine-specific parameters as the bunch length σ_z and the beamstrahlung parameters, Υ and N_γ [66,67]. These latter are given by

$$\Upsilon = \frac{5\alpha N E_e}{6 m_e^3 \sigma_z (\sigma_x + \sigma_y)}, \tag{29}$$

$$N_\gamma = \frac{25\alpha^2 N}{12 m_e (\sigma_x + \sigma_y)\sqrt{1 + \Upsilon^{2/3}}}, \tag{30}$$

where as we mentioned above E_e and σ_z are the energy of the electron and the bunch length, respectively, while m_e are the mass of the electron, N is the number of particles in the bunch, and σ_x and σ_y are the rms beam sizes. The quantity N_γ denotes the average number of photons emitted per electron. Specific values for the beamstrahlung parameters for the future CLIC are presented in Table VII [43,68,69].

Based on all these observations, we must take into account that the sensitivity estimated bounds on anomalous moments $\tilde{\kappa}_{\nu_\tau}$ and $\tilde{d}_{\nu_\tau}$ could be affected by backgrounds coming from ISR and BS. In this regard, Tables VIII and IX illustrate the effects coming from these backgrounds, that is to say including ISR + BS effects on the process $e^+e^- \to \nu_\tau \bar{\nu}_\tau \gamma$. We consider only center-of-mass energy of 3 TeV for the process that is the best obtained on the bounds.

The comparison of the results shown in Tables III and VIII for $\sqrt{s} = 3000$ GeV and $P_{e^-} = P_{e^+} = 0\%$, without and with ISR + BS show that there is a difference in the sensitivity on $\tilde{\kappa}_{\nu_\tau}$ and $\tilde{d}_{\nu_\tau}$ of 23.62%. In the case of Tables VI and IX with $\sqrt{s} = 3000$ GeV, $P_{e^-} = -80\%$ and $P_{e^+} = 60\%$, the difference in the sensitivity without and with ISR + BS is 22.73%. These results show the importance of taking into account the backgrounds coming from ISR and BS in the process $e^+e^- \to \nu_\tau \bar{\nu}_\tau \gamma$.

TABLE IV. Sensitivity estimates on the $\tilde{\kappa}_{\nu_\tau}$ magnetic moment and $\tilde{d}_{\nu_\tau}$ electric dipole moment via the process $e^+e^- \to \nu_\tau\bar{\nu}_\tau\gamma$ for $\sqrt{s} = 380$ GeV, $P_{e^-} = -80\%$ and $P_{e^-} = 60\%$.

90% C.L. $\sqrt{s} = 380$ GeV						
	$\delta_{\rm sys} = 0\%$		$\delta_{\rm sys} = 5\%$		$\delta_{\rm sys} = 10\%$	
$\mathcal{L}(\text{fb}^{-1})$	$\lvert\tilde{\kappa}_{\nu_\tau}\rvert$	$\lvert\tilde{d}_{\nu_\tau}(e\ \text{cm})\rvert$	$\lvert\tilde{\kappa}_{\nu_\tau}\rvert$	$\lvert\tilde{d}_{\nu_\tau}(e\ \text{cm})\rvert$	$\lvert\tilde{\kappa}_{\nu_\tau}\rvert$	$\lvert\tilde{d}_{\nu_\tau}(e\ \text{cm})\rvert$
10	7.563×10^{-6}	1.465×10^{-16}	9.467×10^{-6}	1.592×10^{-16}	1.059×10^{-5}	1.735×10^{-16}
50	5.684×10^{-6}	1.101×10^{-16}	8.485×10^{-6}	1.425×10^{-16}	1.043×10^{-5}	1.644×10^{-16}
100	4.980×10^{-6}	9.651×10^{-17}	8.414×10^{-6}	1.394×10^{-16}	1.041×10^{-5}	1.394×10^{-16}
300	3.993×10^{-6}	7.737×10^{-17}	8.365×10^{-6}	1.372×10^{-16}	1.039×10^{-5}	1.621×10^{-16}
500	3.585×10^{-6}	6.948×10^{-17}	8.355×10^{-6}	1.367×10^{-16}	1.038×10^{-5}	1.619×10^{-16}
95% C.L. $\sqrt{s} = 380$ GeV						
	$\delta_{\rm sys} = 0\%$		$\delta_{\rm sys} = 5\%$		$\delta_{\rm sys} = 10\%$	
$\mathcal{L}(\text{fb}^{-1})$	$\lvert\tilde{\kappa}_{\nu_\tau}\rvert$	$\lvert\tilde{d}_{\nu_\tau}(e\ \text{cm})\rvert$	$\lvert\tilde{\kappa}_{\nu_\tau}\rvert$	$\lvert\tilde{d}_{\nu_\tau}(e\ \text{cm})\rvert$	$\lvert\tilde{\kappa}_{\nu_\tau}\rvert$	$\lvert d_{\nu_\tau}(e\ \text{cm})\rvert$
10	8.018×10^{-6}	1.553×10^{-16}	9.467×10^{-6}	1.834×10^{-16}	1.117×10^{-5}	2.163×10^{-16}
50	6.061×10^{-6}	1.174×10^{-16}	8.975×10^{-6}	1.739×10^{-16}	1.099×10^{-5}	2.130×10^{-16}
100	5.326×10^{-6}	1.032×10^{-16}	8.902×10^{-6}	1.725×10^{-16}	1.097×10^{-5}	2.126×10^{-16}
300	4.289×10^{-6}	8.312×10^{-17}	8.851×10^{-6}	1.715×10^{-16}	1.096×10^{-5}	2.123×10^{-16}
500	3.860×10^{-6}	7.479×10^{-17}	8.841×10^{-6}	1.713×10^{-16}	1.095×10^{-5}	2.122×10^{-16}

H. Cross section of the process $\gamma e^- \to \tau\bar{\nu}_\tau\nu_e$ and dipole moments of the ν_τ with unpolarized electron beam

The future e^+e^- linear colliders are being designed to function also as a γe^- collider with the photon beam generated by the laser-backscattering method; in this mode the flexibility in polarizing both lepton and photon beams will allow unique opportunities to analyze the tau-neutrino properties and interactions. It is therefore conceivable to exploit the sensitivity of this γe^- collider based on e^+e^- linear colliders of center-of-mass energies of 380–3000 GeV. See Refs. [70–73] for a detailed description of the γe^- collider.

On the other hand, although many particles and processes can be produced in the colliders e^+e^- and γe^-, the reactions are different and will give complementary and very valuable information about new physics phenomena, such as is the case of the dipole moments of

TABLE V. Sensitivity estimates on the $\tilde{\kappa}_{\nu_\tau}$ magnetic moment and $\tilde{d}_{\nu_\tau}$ electric dipole moment via the process $e^+e^- \to \nu_\tau\bar{\nu}_\tau\gamma$ for $\sqrt{s} = 1500$ GeV, $P_{e^-} = -80\%$ and $P_{e^+} = 60\%$.

90% C.L. $\sqrt{s} = 1500$ GeV						
	$\delta_{\rm sys} = 0\%$		$\delta_{\rm sys} = 5\%$		$\delta_{\rm sys} = 10\%$	
$\mathcal{L}(\text{fb}^{-1})$	$\lvert\tilde{\kappa}_{\nu_\tau}\rvert$	$\lvert\tilde{d}_{\nu_\tau}(e\ \text{cm})\rvert$	$\lvert\tilde{\kappa}_{\nu_\tau}\rvert$	$\lvert\tilde{d}_{\nu_\tau}(e\ \text{cm})\rvert$	$\lvert\tilde{\kappa}_{\nu_\tau}\rvert$	$\lvert\tilde{d}_{\nu_\tau}(e\ \text{cm})\rvert$
10	1.503×10^{-6}	2.912×10^{-17}	1.654×10^{-6}	3.206×10^{-17}	1.926×10^{-6}	3.732×10^{-17}
100	8.940×10^{-7}	1.732×10^{-17}	1.379×10^{-6}	2.673×10^{-17}	1.805×10^{-6}	3.498×10^{-17}
500	6.085×10^{-7}	1.179×10^{-17}	1.341×10^{-6}	2.600×10^{-17}	1.792×10^{-6}	3.474×10^{-17}
1000	5.140×10^{-7}	9.960×10^{-18}	1.336×10^{-6}	2.590×10^{-17}	1.791×10^{-6}	3.471×10^{-17}
1500	4.654×10^{-7}	9.018×10^{-18}	1.335×10^{-6}	2.587×10^{-17}	1.790×10^{-6}	3.469×10^{-17}
95% C.L. $\sqrt{s} = 1500$ GeV						
	$\delta_{\rm sys} = 0\%$		$\delta_{\rm sys} = 5\%$		$\delta_{\rm sys} = 10\%$	
$\mathcal{L}(\text{fb}^{-1})$	$\lvert\tilde{\kappa}_{\nu_\tau}\rvert$	$\lvert\tilde{d}_{\nu_\tau}(e\ \text{cm})\rvert$	$\lvert\tilde{\kappa}_{\nu_\tau}\rvert$	$\lvert\tilde{d}_{\nu_\tau}(e\ \text{cm})\rvert$	$\lvert\tilde{\kappa}_{\nu_\tau}\rvert$	$\lvert\tilde{d}_{\nu_\tau}(e\ \text{cm})\rvert$
10	1.618×10^{-6}	3.137×10^{-17}	1.779×10^{-6}	3.447×10^{-17}	2.064×10^{-6}	4.000×10^{-17}
100	9.698×10^{-7}	1.879×10^{-17}	1.488×10^{-6}	2.883×10^{-17}	1.937×10^{-6}	3.754×10^{-17}
500	6.620×10^{-7}	1.282×10^{-17}	1.448×10^{-6}	2.886×10^{-17}	1.924×10^{-6}	3.728×10^{-17}
1000	5.596×10^{-7}	1.084×10^{-17}	1.442×10^{-6}	2.795×10^{-17}	1.923×10^{-6}	3.725×10^{-17}
1500	5.069×10^{-7}	9.823×10^{-18}	1.440×10^{-6}	2.792×10^{-17}	1.922×10^{-6}	3.724×10^{-17}

TABLE VI. Sensitivity estimates on the $\tilde{\kappa}_{\nu_\tau}$ magnetic moment and $\tilde{d}_{\nu_\tau}$ electric dipole moment via the process $e^+e^- \to \nu_\tau\bar{\nu}_\tau\gamma$ for $\sqrt{s} = 3000$ GeV, $P_{e^-} = -80\%$ and $P_{e^+} = 60\%$.

90% C.L. $\sqrt{s} = 3000$ GeV						
	$\delta_{\rm sys} = 0\%$		$\delta_{\rm sys} = 5\%$		$\delta_{\rm sys} = 10\%$	
$\mathcal{L}(\text{fb}^{-1})$	$\lvert\tilde{\kappa}_{\nu_\tau}\rvert$	$\lvert\tilde{d}_{\nu_\tau}(e\ \text{cm})\rvert$	$\lvert\tilde{\kappa}_{\nu_\tau}\rvert$	$\lvert\tilde{d}_{\nu_\tau}(e\ \text{cm})\rvert$	$\lvert\tilde{\kappa}_{\nu_\tau}\rvert$	$\lvert\tilde{d}_{\nu_\tau}(e\ \text{cm})\rvert$
100	4.609×10^{-7}	9.276×10^{-18}	5.735×10^{-7}	1.160×10^{-17}	7.284×10^{-7}	1.475×10^{-17}
500	3.116×10^{-7}	6.281×10^{-18}	5.235×10^{-7}	1.064×10^{-17}	7.085×10^{-7}	1.437×10^{-17}
1000	2.628×10^{-7}	5.299×10^{-18}	5.161×10^{-7}	1.049×10^{-17}	7.059×10^{-7}	1.432×10^{-17}
2000	2.214×10^{-7}	4.465×10^{-18}	5.122×10^{-7}	1.042×10^{-17}	7.046×10^{-7}	1.429×10^{-17}
3000	2.002×10^{-7}	4.039×10^{-18}	5.109×10^{-7}	1.039×10^{-17}	7.041×10^{-7}	1.428×10^{-17}
95% C.L. $\sqrt{s} = 3000$ GeV						
	$\delta_{\rm sys} = 0\%$		$\delta_{\rm sys} = 5\%$		$\delta_{\rm sys} = 10\%$	
$\mathcal{L}(\text{fb}^{-1})$	$\lvert\tilde{\kappa}_{\nu_\tau}\rvert$	$\lvert\tilde{d}_{\nu_\tau}(e\ \text{cm})\rvert$	$\lvert\tilde{\kappa}_{\nu_\tau}\rvert$	$\lvert\tilde{d}_{\nu_\tau}(e\ \text{cm})\rvert$	$\lvert\tilde{\kappa}_{\nu_\tau}\rvert$	$\lvert\tilde{d}_{\nu_\tau}(e\ \text{cm})\rvert$
100	5.010×10^{-7}	1.007×10^{-17}	6.223×10^{-7}	1.258×10^{-17}	7.883×10^{-7}	1.595×10^{-17}
500	3.394×10^{-7}	6.840×10^{-18}	5.686×10^{-7}	1.154×10^{-17}	7.671×10^{-7}	1.554×10^{-17}
1000	2.863×10^{-7}	5.773×10^{-18}	5.605×10^{-7}	1.139×10^{-17}	7.642×10^{-7}	1.549×10^{-17}
2000	2.413×10^{-7}	4.867×10^{-18}	5.564×10^{-7}	1.131×10^{-17}	7.628×10^{-7}	1.546×10^{-17}
3000	2.183×10^{-7}	4.403×10^{-18}	5.549×10^{-7}	1.128×10^{-17}	7.623×10^{-7}	1.545×10^{-17}

TABLE VII. Benchmark parameters of the CLIC related to the beamstrahlung [43,68,69].

CLIC parameters	$\sqrt{s} = 3$ TeV
N(10^9)	3.72
σ_x(nm)	40
σ_y(nm)	1
$\sigma_z(\mu\text{m})$	44
Υ	5.49
N_γ	1.92

the tau-neutrino which we study through the process $\gamma e^- \to \tau\bar{\nu}_\tau\nu_e$. To carry out this task, we use the gauge-invariant operators of dimension six leading to electromagnetic vertex $\nu_\tau\bar{\nu}_\tau\gamma$ given by Eq. (4). Furthermore, it is worth mentioning that the additional coupling $W\tau\nu_\tau$ can contribute to the dipole moments of the tau-neutrino. In this case, the operators $\mathcal{O}_{\nu_l W}$ and $\tilde{\mathcal{O}}_{\nu_l W}$ given in Eqs. (9) and (11) also generate an additional coupling between the W, τ and the ν_τ. This additional $W\tau\nu_\tau$ coupling is proportional to the

TABLE VIII. Sensitivity estimates on the $\tilde{\kappa}_{\nu_\tau}$ magnetic moment and $\tilde{d}_{\nu_\tau}$ electric dipole moment via the process $e^+e^- \to \nu_\tau\bar{\nu}_\tau\gamma$ for $\sqrt{s} = 3000$ GeV and $P_{e^-} = P_{e^+} = 0\%$, including ISR + BS effects.

90% C.L. $\sqrt{s} = 3000$ GeV						
	$\delta_{\rm sys} = 0\%$		$\delta_{\rm sys} = 5\%$		$\delta_{\rm sys} = 10\%$	
$\mathcal{L}(\text{fb}^{-1})$	$\lvert\tilde{\kappa}_{\nu_\tau}\rvert$	$\lvert\tilde{d}_{\nu_\tau}(e\ \text{cm})\rvert$	$\lvert\tilde{\kappa}_{\nu_\tau}\rvert$	$\lvert\tilde{d}_{\nu_\tau}(e\ \text{cm})\rvert$	$\lvert\tilde{\kappa}_{\nu_\tau}\rvert$	$\lvert\tilde{d}_{\nu_\tau}(e\ \text{cm})\rvert$
100	6.288×10^{-7}	1.218×10^{-17}	7.902×10^{-7}	1.531×10^{-17}	1.001×10^{-6}	1.941×10^{-17}
500	4.274×10^{-7}	8.282×10^{-18}	7.279×10^{-7}	1.410×10^{-17}	9.778×10^{-7}	1.894×10^{-17}
1000	3.609×10^{-7}	6.993×10^{-18}	7.186×10^{-7}	1.392×10^{-17}	9.747×10^{-7}	9.747×10^{-17}
2000	3.043×10^{-7}	5.898×10^{-18}	7.139×10^{-7}	1.383×10^{-17}	9.731×10^{-7}	9.731×10^{-17}
3000	2.754×10^{-7}	5.336×10^{-18}	7.122×10^{-7}	1.380×10^{-17}	9.725×10^{-7}	9.725×10^{-17}
95% C.L. $\sqrt{s} = 3000$ GeV						
	$\delta_{\rm sys} = 0\%$		$\delta_{\rm sys} = 5\%$		$\delta_{\rm sys} = 10\%$	
$\mathcal{L}(\text{fb}^{-1})$	$\lvert\tilde{\kappa}_{\nu_\tau}\rvert$	$\lvert\tilde{d}_{\nu_\tau}(e\ \text{cm})\rvert$	$\lvert\tilde{\kappa}_{\nu_\tau}\rvert$	$\lvert\tilde{d}_{\nu_\tau}(e\ \text{cm})\rvert$	$\lvert\tilde{\kappa}_{\nu_\tau}\rvert$	$\lvert\tilde{d}_{\nu_\tau}(e\ \text{cm})\rvert$
100	6.825×10^{-7}	1.322×10^{-17}	8.555×10^{-7}	1.657×10^{-17}	1.080×10^{-6}	2.094×10^{-17}
500	4.651×10^{-7}	9.013×10^{-18}	7.888×10^{-7}	1.528×10^{-17}	1.055×10^{-6}	2.045×10^{-17}
1000	3.930×10^{-7}	7.615×10^{-18}	7.789×10^{-7}	1.509×10^{-17}	1.052×10^{-6}	2.038×10^{-17}
2000	3.316×10^{-7}	6.426×10^{-18}	7.738×10^{-7}	1.499×10^{-17}	1.050×10^{-6}	2.035×10^{-17}
3000	3.001×10^{-7}	5.336×10^{-18}	7.720×10^{-7}	1.496×10^{-17}	1.049×10^{-7}	2.034×10^{-17}

TABLE IX. Sensitivity estimates on the $\tilde{\kappa}_{\nu_\tau}$ magnetic moment and $\tilde{d}_{\nu_\tau}$ electric dipole moment via the process $e^+e^- \to \nu_\tau\bar{\nu}_\tau\gamma$ for $\sqrt{s} = 3000$ GeV, $P_{e^-} = -80\%$ and $P_{e^+} = 60\%$, including ISR + BS effects.

90% C.L. $\sqrt{s} = 3000$ GeV						
	$\delta_{\rm sys} = 0\%$		$\delta_{\rm sys} = 5\%$		$\delta_{\rm sys} = 10\%$	
$\mathcal{L}(\text{fb}^{-1})$	$\lvert\tilde{\kappa}_{\nu_\tau}\rvert$	$\lvert\tilde{d}_{\nu_\tau}(e\ \text{cm})\rvert$	$\lvert\tilde{\kappa}_{\nu_\tau}\rvert$	$\lvert\tilde{d}_{\nu_\tau}(e\ \text{cm})\rvert$	$\lvert\tilde{\kappa}_{\nu_\tau}\rvert$	$\lvert\tilde{d}_{\nu_\tau}(e\ \text{cm})\rvert$
100	5.938×10^{-7}	1.150×10^{-17}	8.196×10^{-7}	1.588×10^{-17}	1.149×10^{-6}	2.227×10^{-17}
500	4.027×10^{-7}	7.804×10^{-18}	7.783×10^{-7}	1.508×10^{-17}	1.051×10^{-6}	2.037×10^{-17}
1000	3.398×10^{-7}	6.585×10^{-18}	7.726×10^{-7}	1.497×10^{-17}	1.049×10^{-6}	2.033×10^{-17}
2000	2.865×10^{-7}	5.551×10^{-18}	7.697×10^{-7}	1.491×10^{-17}	1.048×10^{-6}	2.031×10^{-17}
3000	2.591×10^{-7}	5.022×10^{-18}	7.687×10^{-7}	1.489×10^{-17}	1.048×10^{-6}	2.031×10^{-17}
95% C.L. $\sqrt{s} = 3000$ GeV						
	$\delta_{\rm sys} = 0\%$		$\delta_{\rm sys} = 5\%$		$\delta_{\rm sys} = 10\%$	
$\mathcal{L}(\text{fb}^{-1})$	$\lvert\tilde{\kappa}_{\nu_\tau}\rvert$	$\lvert\tilde{d}_{\nu_\tau}(e\ \text{cm})\rvert$	$\lvert\tilde{\kappa}_{\nu_\tau}\rvert$	$\lvert\tilde{d}_{\nu_\tau}(e\ \text{cm})\rvert$	$\lvert\tilde{\kappa}_{\nu_\tau}\rvert$	$\lvert\tilde{d}_{\nu_\tau}(e\ \text{cm})\rvert$
100	6.449×10^{-7}	1.249×10^{-17}	8.871×10^{-7}	1.719×10^{-17}	1.149×10^{-6}	2.227×10^{-17}
500	4.384×10^{-7}	8.496×10^{-18}	8.430×10^{-7}	1.633×10^{-17}	1.133×10^{-6}	2.197×10^{-17}
1000	3.702×10^{-7}	7.173×10^{-18}	8.369×10^{-7}	1.621×10^{-17}	1.131×10^{-6}	2.193×10^{-17}
2000	3.122×10^{-7}	6.050×10^{-18}	8.338×10^{-7}	1.615×10^{-17}	1.130×10^{-6}	2.191×10^{-17}
3000	2.825×10^{-7}	5.474×10^{-18}	8.327×10^{-7}	1.613×10^{-17}	1.130×10^{-6}	2.190×10^{-17}

combination $\tilde{\kappa}'_{\nu_\tau} = F_1\tilde{\kappa}_{\nu_\tau} - F_2\tilde{\kappa}^W_{\nu_\tau}$ and $\tilde{d}'_{\nu_\tau} = G_1\tilde{d}_{\nu_\tau} + G_2\tilde{d}^W_{\nu_\tau}$, where $\tilde{\kappa}_{\nu_\tau}$ and $\tilde{d}_{\nu_\tau}$ come from the contribution of the electromagnetic vertex $\nu_\tau\bar{\nu}_\tau\gamma$, while $\tilde{\kappa}^W_{\nu_\tau}$ and $\tilde{d}^W_{\nu_\tau}$ correspond to the electroweak vertex $W\tau\nu_\tau$. $F_1(G_1)$ and $F_2(G_2)$ contain $\sin\theta_W$ and $\cos\theta_W$ factors. The dynamics of the process $\gamma e^- \to \tau\bar{\nu}_\tau\nu_e$ is modified both by nonstandard terms proportional to $\tilde{\kappa}_{\nu_\tau}$ and $\tilde{d}_{\nu_\tau}$, as well as by contributions generated by the new $W\tau\nu_\tau$ coupling, which are proportional to $\tilde{\kappa}'_{\nu_\tau}$ and $\tilde{d}'_{\nu_\tau}$. At this time, we do not contemplate the new anomalous $W\tau\nu_\tau$ coupling in our study. Figure 12 shows the Feynman diagrams corresponding to said process. We evaluate the total cross section of $\gamma e^- \to \tau\bar{\nu}_\tau\nu_e$ as a function of the anomalous factors $\tilde{\kappa}_{\nu_\tau}$, $\tilde{d}_{\nu_\tau}$ and tau lepton decays hadronic and leptonic modes are considered.

In order to evaluate the total cross section $\sigma(\gamma e^- \to \tau\bar{\nu}_\tau\nu_e)$ and to probe the dipole moments $\tilde{\kappa}_{\nu_\tau}$ and $\tilde{d}_{\nu_\tau}$, we examine the potential of the CLIC based γe^- collider with the main parameters given by $\sqrt{s} = 380$, 1500, 3000 GeV and $\mathcal{L} = 10$, 50, 100, 200, 500, 1000, 1500, 2000, 3000 fb^{-1}. In addition, in order to suppress the backgrounds and optimize the signal sensitivity, we impose for our study the following kinematic basic acceptance cuts for $\tau\bar{\nu}_\tau\nu_e$ events at the CLIC:

$$\begin{aligned} &\text{Cut-1:}\ p_T^\nu > 15\ \text{GeV}, \\ &\text{Cut-2:}\ |\eta^\tau| < 2.37, \\ &\text{Cut-3:}\ p_T^\tau > 20\ \text{GeV}, \end{aligned} \tag{31}$$

where in Eq. (31), $p_T^{\nu,\tau}$ is the transverse momentum of the final state particles and η^τ is the pseudorapidity which reduces the contamination from other particles misidentified as tau.

Furthermore, to study the sensitivity to the parameters of the $\gamma e^- \to \tau\bar{\nu}_\tau\nu_e$ process we use the chi-squared function. The χ^2 function is defined in Eq. (24). However, in the case of the $\gamma e^- \to \tau\bar{\nu}_\tau\nu_e$ process, the number of events is given

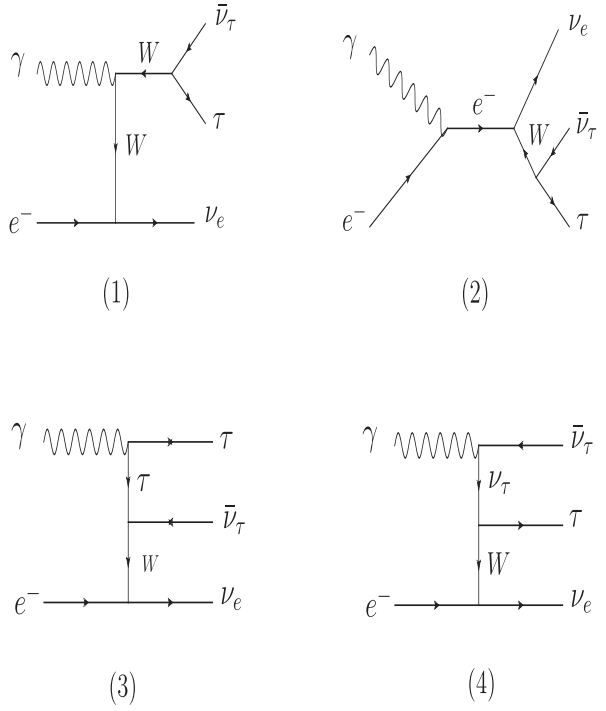

FIG. 12. The Feynman diagrams contributing to the process $\gamma e^- \to \tau\bar{\nu}_\tau\nu_e$.

by $N_{SM} = \mathcal{L}_{int} \times \sigma_{SM} \times BR$, where $\mathcal{L}_{int}$ is the integrated CLIC luminosity. The main tau-decay branching ratios are given in Ref. [26]. In addition, as the tau-lepton decays roughly 35% of the time leptonically and 65% of the time to one or more hadrons, then for the signal the following cases are considered: (a) only the leptonic decay channel of the tau-lepton; (b) only the hadronic decay channel of the tau-lepton.

Systematic uncertainties arise due to many factors when identifying to the tau-lepton. Tau tagging efficiencies have been studied using the International Large Detector (ILD) [74], a proposed detector concept for the International Linear Collider (ILC). However, we do not have any CLIC reports [75,76] to know exactly what the systematic uncertainties are for our processes; we can assume some of their general values. Due to these difficulties, tau identification efficiencies are always calculated for specific processes, luminosity, and kinematic parameters. These studies are currently being carried out by various groups for selected productions. For realistic efficiency, we need a detailed study for our specific process and kinematic parameters. For all of these reasons, kinematic cuts contain some general values chosen by lepton identification detectors and efficiency is therefore considered within systematic errors. It may be assumed that this accelerator will be built in the coming years and the systematic uncertainties will be lower as detector technology develops in the future.

It is also important to consider the impact of the polarization electron beam on the collider. On this, the CLIC baseline design supposes that the electron beams can be polarized up to $\mp 80\%$ [65,77]. By choosing different beam polarizations it is possible to enhance or suppress different physical processes. Furthermore, in the study of the process $\gamma e^- \to \tau\bar{\nu}_\tau\nu_e$ the polarization electron beam may lead to a reduction of the measurement uncertainties, either by increasing the signal cross section, therefore reducing the statistical uncertainty, or by suppressing important backgrounds.

For the γe^- collider, the most promising mechanism to generate energetic photon beam in a linear collider is Compton backscattering. The photon beams are generated by the Compton backscattered of incident electron and laser beams just before the interaction point. The total cross sections of the process $\gamma e^- \to \tau\bar{\nu}_\tau\nu_e$ are

$$\sigma = \int f_{\gamma/e}(x) d\hat{\sigma} dE_1. \tag{32}$$

In this equation, the spectrum of Compton backscattered photons [70,71] is given by

$$f_\gamma(y) = \frac{1}{g(\zeta)}\left[1 - y + \frac{1}{1-y} - \frac{4y}{\zeta(1-y)} + \frac{4y^2}{\zeta^2(1-y)^2}\right], \tag{33}$$

where

$$g(\zeta) = \left(1 - \frac{4}{\zeta} - \frac{8}{\zeta^2}\right)\log(\zeta+1) + \frac{1}{2} + \frac{8}{\zeta} - \frac{1}{2(\zeta+1)^2}, \tag{34}$$

with

$$y = \frac{E_\gamma}{E_e}, \qquad \zeta = \frac{4E_0E_e}{M_e^2}, \qquad y_{max} = \frac{\zeta}{1+\zeta}. \tag{35}$$

Here, E_0 and E_e are energy of the incoming laser photon and initial energy of the electron beams before Compton backscattering and E_γ is the energy of the backscattered photon. The maximum value of y reaches 0.83 when $\zeta = 4.8$.

As the first observable, we consider the total cross section. Figures 13 and 14 summarize the total cross section of the process $\gamma e^- \to \tau\bar{\nu}_\tau\nu_e$ with unpolarized electron beams and as a function of the anomalous couplings $\tilde{\kappa}_{\nu_\tau}(\tilde{d}_{\nu_\tau})$. We use the three stages of the center-of-mass energy of the CLIC,

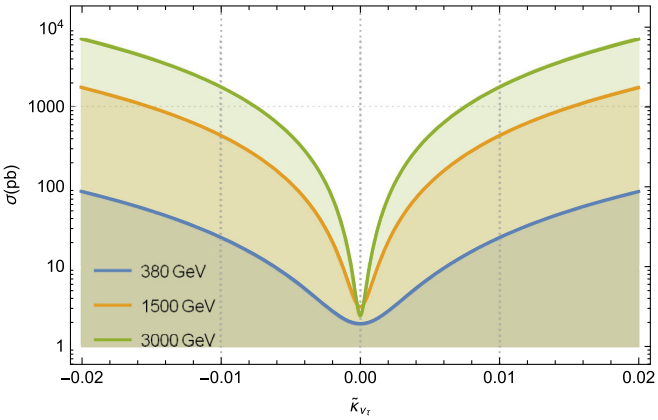

FIG. 13. The total cross section of the process $\gamma e^- \to \tau\bar{\nu}_\tau\nu_e$ as a function of the anomalous coupling $\tilde{\kappa}_{\nu_\tau}$ for three different center-of-mass energies $\sqrt{s} = 380$, 1500, 3000 GeV.

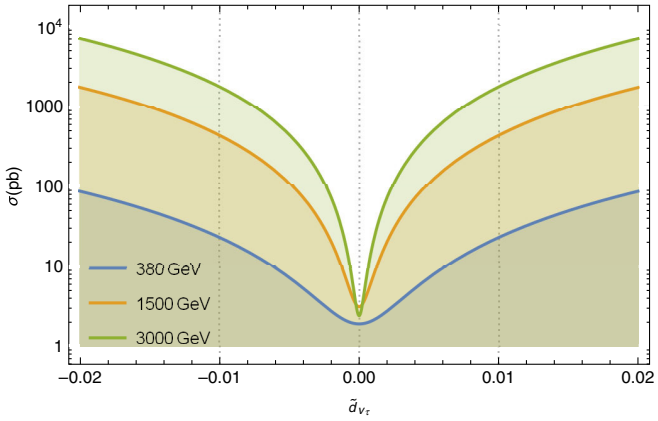

FIG. 14. Same as in Fig. 13, but for $\tilde{d}_{\nu_\tau}$.

that is to say $\sqrt{s} = 380$, 1500, 3000 GeV and $\mathcal{L} = 10$, 50, 100, 200, 500, 1000, 1500, 2000, 3000 fb^{-1}. The total cross section clearly shows a strong dependence with respect to the anomalous parameters $\tilde{\kappa}_{\nu_\tau}$, $\tilde{d}_{\nu_\tau}$, as well as with the center-of-mass energy of the collider $\sqrt{s}$.

The total cross section of the process $\gamma e^- \to \tau\bar{\nu}_\tau\nu_e$ as a function of $\tilde{\kappa}_{\nu_\tau}$ and $\tilde{d}_{\nu_\tau}$ with the benchmark parameters of the CLIC is shown in Figs. 15–17. The total cross section increases with the increase in the center-of-mass energy of the collider and strongly depends on anomalous couplings $\tilde{\kappa}_{\nu_\tau}$ and $\tilde{d}_{\nu_\tau}$.

In order to investigate the signal more comprehensively, we show the bound contours depending on integrated luminosity at the 95% C.L. on the $(\tilde{\kappa}_{\nu_\tau}, \tilde{d}_{\nu_\tau})$ plane for $\sqrt{s} = 380$, 1500, 3000 GeV in Figs. 18–20. At 95% C.L. and $\sqrt{s} = 3000$ GeV, we can see that the correlation region of $\tilde{\kappa}_{\nu_\tau} \in [-2.5; 2.5] \times 10^{-5}$ and $\tilde{d}_{\nu_\tau} \in [-2.5; 2.5] \times 10^{-5}$ can be excluded with integrate luminosity $\mathcal{L} = 100$ fb^{-1}. If the integrated luminosity is increased to $\mathcal{L} = 3000$ fb^{-1}, the excluded region will expand into $\tilde{\kappa}_{\nu_\tau} \in [-1, 1] \times 10^{-5}$ and $\tilde{d}_{\nu_\tau} \in [-1, 1] \times 10^{-5}$.

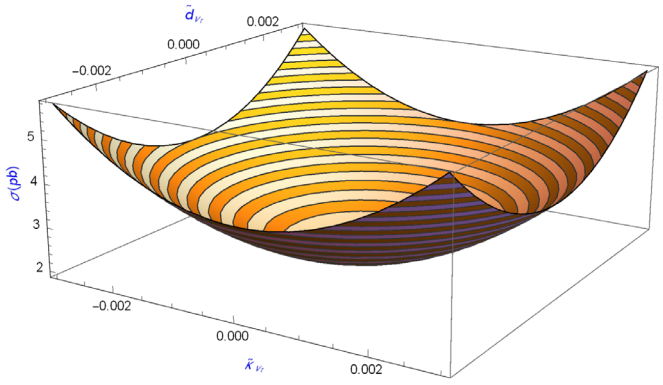

FIG. 15. The total cross sections of the process $\gamma e^- \to \tau\bar{\nu}_\tau\nu_e$ as a function of $\tilde{\kappa}_{\nu_\tau}$ and $\tilde{d}_{\nu_\tau}$ for center-of-mass energy of $\sqrt{s} = 380$ GeV.

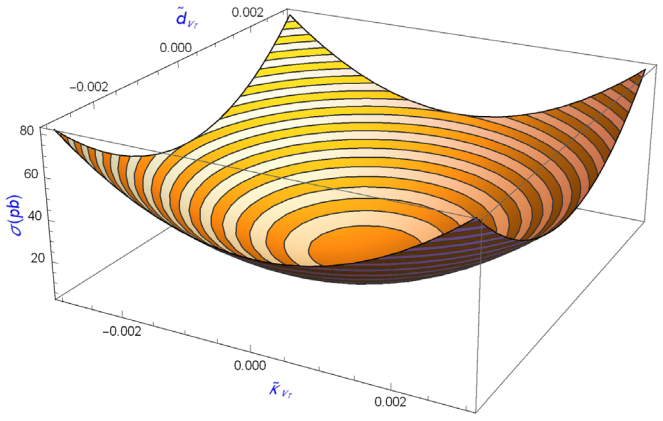

FIG. 16. Same as in Fig. 15, but for $\sqrt{s} = 1500$ GeV.

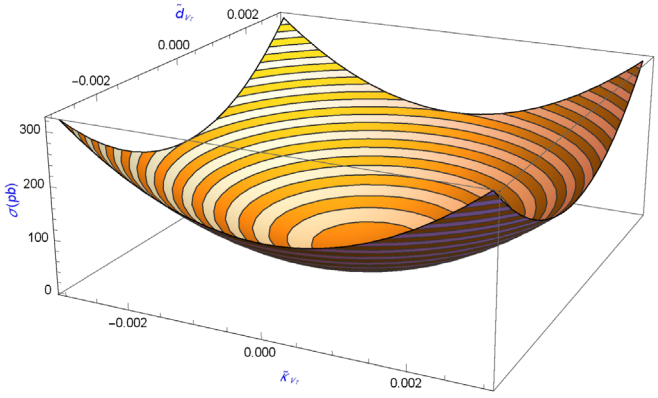

FIG. 17. Same as in Fig. 15, but for $\sqrt{s} = 3000$ GeV.

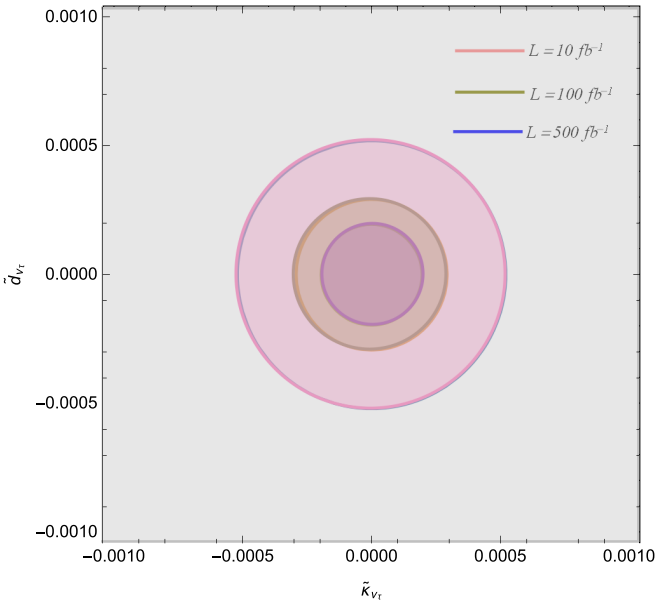

FIG. 18. Bounds contours at the 95% C.L. in the $\tilde{\kappa}_{\nu_\tau} - \tilde{d}_{\nu_\tau}$ plane for the process $\gamma e^- \to \tau\bar{\nu}_\tau\nu_e$ with the $\delta_{\text{sys}} = 0\%$ and for center-of-mass energy of $\sqrt{s} = 380$ GeV.

I. Cross section of the process $\gamma e^- \to \tau\bar{\nu}_\tau\nu_e$ and dipole moments of the ν_τ with polarized electron beam

We consider the total cross section of the process $\gamma e^- \to \tau\bar{\nu}_\tau\nu_e$ as a function of the anomalous factors $\tilde{\kappa}_{\nu_\tau}(\tilde{d}_{\nu_\tau})$ and we perform our analysis for the CLIC running at center-of-mass energies and luminosities of $\sqrt{s} = 380$, 1500, 3000 GeV and $\mathcal{L} = 10$, 50, 100, 200, 500, 1000, 1500, 2000, 3000 fb^{-1}. Furthermore, in our analysis we consider the baseline expectation of an −80% left-polarized electron beam. As expected, the polarization hugely improves the total cross section as is shown in Figs. 21 and 22. The total cross section is increased from about $\sigma = 8 \times 10^3$ pb with unpolarized electron beam (see Figs. 13 and 14) to about $\sigma = 1.5 \times 10^4$ pb with polarized electron beam (see Figs. 21 and 22), respectively,

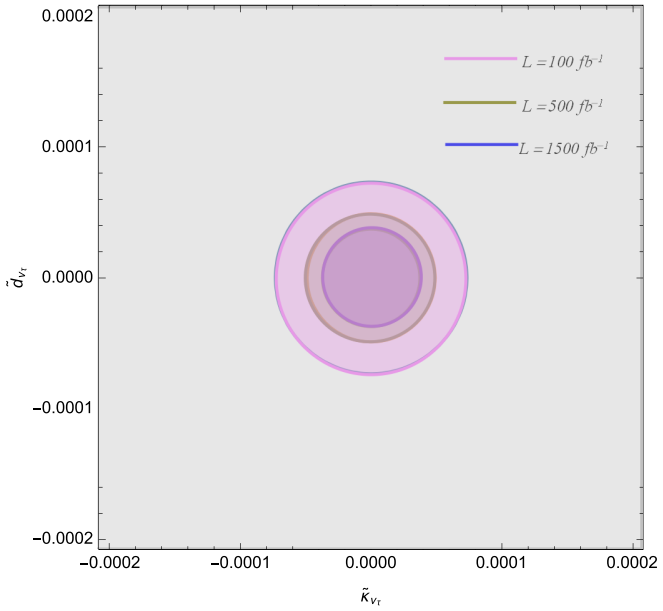

FIG. 19. Same as in Fig. 18, but for $\sqrt{s} = 1500$ GeV.

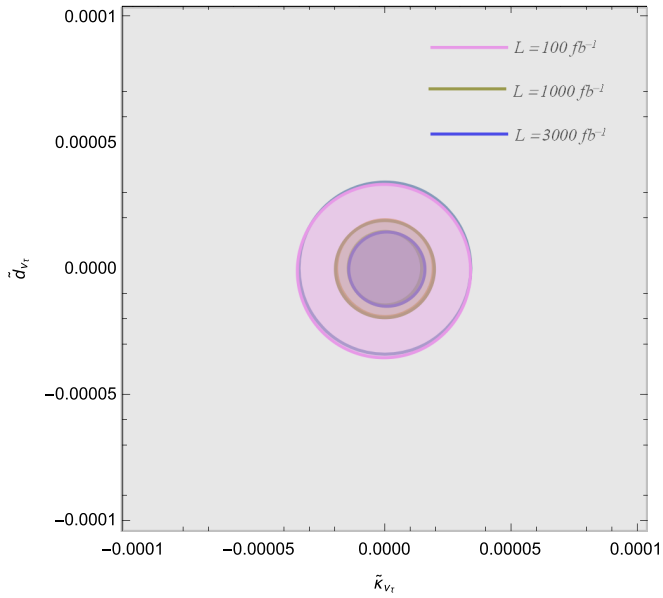

FIG. 20. Same as in Fig. 18, but for $\sqrt{s} = 3000$ GeV.

enhancing the statistic. The increase of the total cross section of the process $\gamma e^- \to \tau\bar{\nu}_\tau\nu_e$ for the polarized case is approximately the double of the unpolarized case. The reason why the cross section of the polarized process is larger than the cross section of the unpolarized process is due to the structure of the $We^-\nu_{e^-}$ vertex. The advantage of beam polarization is evident when compared to the corresponding unpolarized case.

In Figs. 23 and 24 we plot the χ^2 versus $\tilde{\kappa}_{\nu_\tau}(\tilde{d}_{\nu_\tau})$ with unpolarized $P_{e^-} = 0\%$ and polarized $P_{e^-} = -80\%$ electron beam and 95% C.L. We plot the curves for each case, for

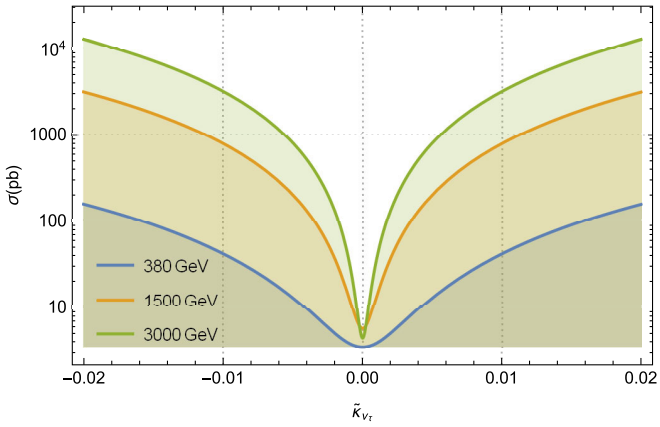

FIG. 21. Same as in Fig. 13, but with polarized electron beam $P_e = -80\%$.

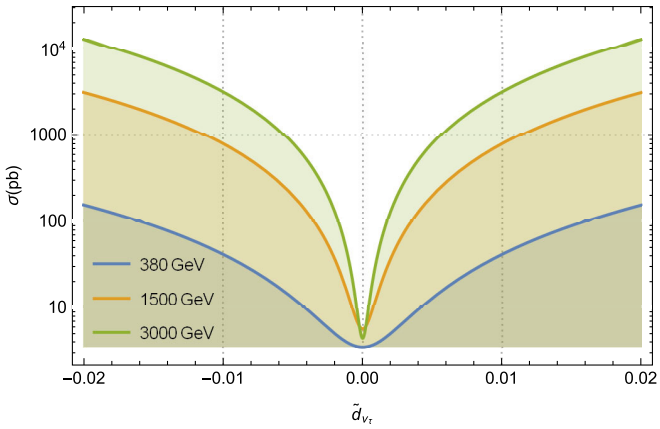

FIG. 22. Same as in Fig. 14, but with polarized electron beam $P_e = -80\%$.

which we have divided the interval of $\tilde{\kappa}_{\nu_\tau}(\tilde{d}_{\nu_\tau})$ into several bins. From these figures we can see that the effect of the polarized beam is to reduce the interval of definition of $\tilde{\kappa}_{\nu_\tau} \in [-2;2] \times 10^{-5}$ (unpolarized case) to $\tilde{\kappa}_{\nu_\tau} \in [-1.65; 1.65] \times 10^{-5}$ (polarized case) and $\tilde{d}_{\nu_\tau} \in [-2;2] \times 10^{-5}$ (unpolarized case) to $\tilde{d}_{\nu_\tau} \in [-1.65; 1.65] \times 10^{-5}$ (polarized case), respectively.

Another important observable is the transverse momentum p_T^τ of the tau lepton, the pseudorapidity η^τ is also important, these quantities are shown in Figs. 25 and 26. In both cases, the tau-lepton pseudorapidity and the transverse momentum are for the SM, SM-polarized beam, $\tilde{\kappa}_{\nu_\tau}$ and $\tilde{\kappa}_{\nu_\tau}$-polarized beam. From Fig. 25, the $d\sigma/d\eta$ clearly shows a strong dependence with respect to the pseudorapidity, as well as with the factors $\tilde{\kappa}_{\nu_\tau}$ and $\tilde{\kappa}_{\nu_\tau}$-polarized beam. In the case of Fig. 26, the distribution $d\sigma/dp_T$(pb/GeV) decreases with the increase of p_T for the SM and the SM-polarized beam, while for $\tilde{\kappa}_{\nu_\tau}$ and $\tilde{\kappa}_{\nu_\tau}$-polarized beam have the opposite effect. These

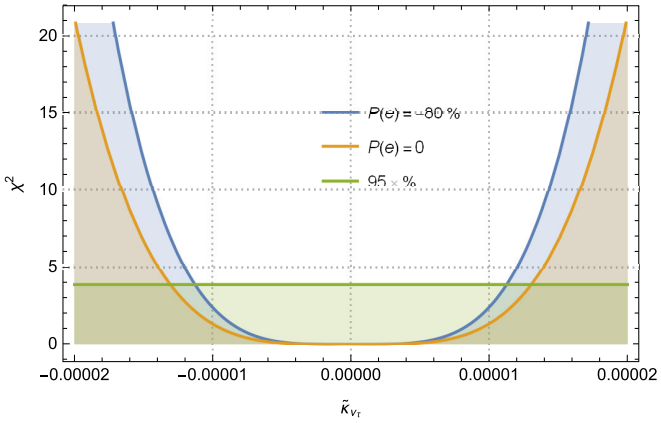

FIG. 23. χ^2 as a function of $\tilde{\kappa}_{\nu_\tau}$ for the total cross section of the process $\gamma e^- \to \tau\bar{\nu}_\tau\nu_e$.

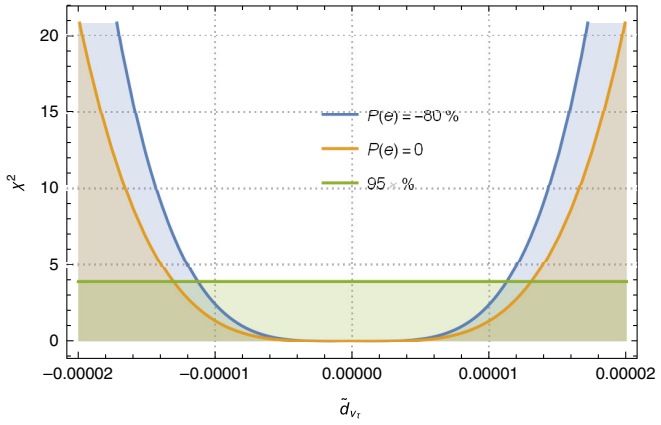

FIG. 24. Same as in Fig. 23, but for $\tilde{d}_{\nu_\tau}$.

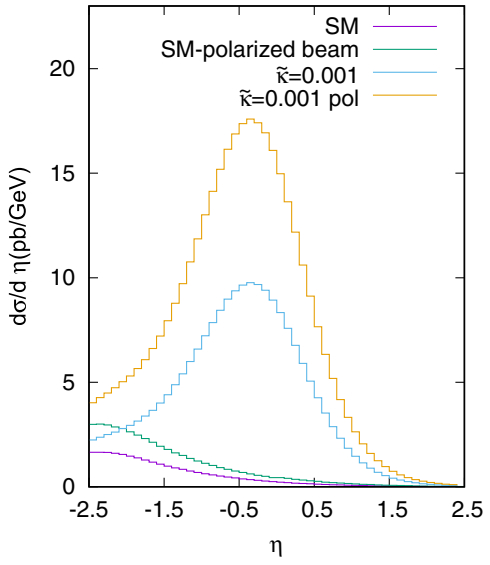

FIG. 25. Generated tau-lepton pseudorapidity distribution for $\gamma e^- \to \tau\bar{\nu}_\tau\nu_e$. The distributions are for SM (SM-polarized beam) and $\tilde{\kappa}_{\nu_\tau}$ ($\tilde{\kappa}_{\nu_\tau}$-polarized beam).

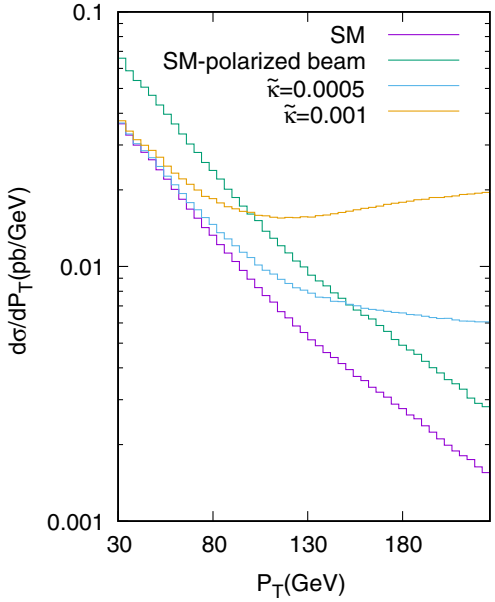

FIG. 26. Same as in Fig. 25, but for p_T.

distributions clearly show great sensitivity with respect to the anomalous factor $\tilde{\kappa}_{\nu_\tau}$ for the cases with unpolarized and polarized electron beam. The analysis of these distributions is important to be able to discriminate the basic acceptance cuts for $\tau\bar{\nu}_\tau\nu_e$ events at the CLIC.

J. 90% C.L and 95% C.L bounds on the anomalous ν_τMM and ν_τEDM with unpolarized and polarized electron beams

In the following we will refer to the anomalous ν_τMM and ν_τEDM. From Feynman diagrams for the process $\gamma e^- \to \tau\bar{\nu}_\tau\nu_e$ given in Fig. 12, for the estimation of the sensitivity on the anomalous dipole moments, we consider the following scenarios: (a) unpolarized electrons beams $P_{e^-} = 0\%$ and we considered only the leptonic decay channel of the tau-lepton; (b) polarized electrons beams $P_{e^-} = -80\%$, and we considered only the leptonic decay channel of the tau-lepton; (c) unpolarized electrons beams $P_{e^-} = 0\%$ and we considered only the hadronic decay channel of the tau-lepton; (d) polarized electrons beams $P_{e^-} = -80\%$ and we considered only the hadronic decay channel of the tau-lepton; (e) unpolarized electrons beams $P_{e^-} = 0\%$ and we considered only the leptonic decay channel of the tau-lepton, including ISR + BS effects; (f) polarized electrons beams $P_{e^-} = -80\%$ and we considered only the hadronic decay channel of the tau-lepton, including ISR + BS effects. For all these scenarios, we consider the energies and luminosities for the future CLIC $\sqrt{s} = 380, 1500, 3000$ GeV and $\mathcal{L} = 10, 50, 100, 200, 500, 1000, 1500, 2000, 3000$ fb^{-1}. In addition, we impose kinematic cuts on p_T^ν, p_T^τ and η^τ to suppress the backgrounds and to optimize the signal sensitivity [see Eq. (31)], we also consider the systematic uncertainties

TABLE X. Limits on the $\tilde{\kappa}_{\nu_\tau}$ magnetic moment and $\tilde{d}_{\nu_\tau}$ electric dipole moment via the process $\gamma e^- \to \tau\bar{\nu}_\tau\nu_e$ (γ is the Compton backscattering photon) for $P_{e^-} = 0\%$, and we considered only the leptonic decay channel of the tau-lepton.

90% C.L. $\sqrt{s} = 1500$ GeV		
$\mathcal{L}(\text{fb}^{-1})$	$\lvert\tilde{\kappa}_{\nu_\tau}\rvert$ (10^{-7})	$\lvert\tilde{d}_{\nu_\tau}\rvert(10^{-17})(e$ cm$)$
100	16.810	3.258
200	14.130	2.739
500	11.240	2.178
1000	9.455	1.832
1500	8.544	1.655
$\delta_{\text{sys}} = 5\%$	6.860×10^{-6}	1.322×10^{-16}
$\delta_{\text{sys}} = 10\%$	9.701×10^{-6}	1.879×10^{-16}
95% C.L. $\sqrt{s} = 1500$ GeV		
100	18.340	3.554
200	15.420	2.989
500	12.260	2.377
1000	10.310	1.999
1500	9.3210	1.806
$\delta_{\text{sys}} = 5\%$	7.484×10^{-6}	1.450×10^{-16}
$\delta_{\text{sys}} = 10\%$	10.580×10^{-6}	2.051×10^{-16}

TABLE XII. Limits on the $\tilde{\kappa}_{\nu_\tau}$ magnetic moment and $\tilde{d}_{\nu_\tau}$ electric dipole moment via the process $\gamma e^- \to \tau\bar{\nu}_\tau\nu_e$ (γ is the Compton backscattering photon) for $P_{e^-} = -80\%$, and we considered only the leptonic decay channel of the tau-lepton.

90% C.L. $\sqrt{s} = 1500$ GeV		
$\mathcal{L}(\text{fb}^{-1})$	$\lvert\tilde{\kappa}_{\nu_\tau}\rvert$ (10^{-7})	$\lvert\tilde{d}_{\nu_\tau}\rvert(10^{-17})(e$ cm$)$
100	14.520	2.814
200	12.210	2.366
500	9.713	1.882
1000	8.167	1.582
1500	7.380	1.430
$\delta_{\text{sys}} = 5\%$	6.865×10^{-6}	1.330×10^{-16}
$\delta_{\text{sys}} = 10\%$	9.709×10^{-6}	1.881×10^{-16}
95% C.L. $\sqrt{s} = 1500$ GeV		
100	15.840	3.070
200	13.320	2.582
500	10.590	2.053
1000	8.911	1.726
1500	8.052	1.560
$\delta_{\text{sys}} = 5\%$	7.491×10^{-6}	1.451×10^{-16}
$\delta_{\text{sys}} = 10\%$	10.590×10^{-6}	2.052×10^{-16}

$\delta_{\text{sys}} = 0\%$, 5%, 10%. The achievable precision in the determination of the sensibility on $\tilde{\kappa}_{\nu_\tau}$ and $\tilde{d}_{\nu_\tau}$ is summarized in Tables X–XIX.

The best sensitivity achieved for the anomalous $\tilde{\kappa}_{\nu_\tau}$ and the $\tilde{d}_{\nu_\tau}$ for the case of $P_{e^-} = 0\%$, and considering only the leptonic decay channel of the tau-lepton, are $|\tilde{\kappa}_{\nu_\tau}| = 3.649 \times 10^{-7}$ and $|\tilde{d}_{\nu_\tau}(e\text{ cm})| = 7.072 \times 10^{-18}$. In the case of $P_{e^-} = -80\%$, and considering only the leptonic decay channel of the tau-lepton, the sensitivity estimates are $|\tilde{\kappa}_{\nu_\tau}| = 3.152 \times 10^{-7}$ and $|\tilde{d}_{\nu_\tau}(e\text{ cm})| = 6.108 \times 10^{-18}$.

TABLE XI. Limits on the $\tilde{\kappa}_{\nu_\tau}$ magnetic moment and $\tilde{d}_{\nu_\tau}$ electric dipole moment via the process $\gamma e^- \to \tau\bar{\nu}_\tau\nu_e$ (γ is the Compton backscattering photon) for $P_{e^-} = 0\%$, and we considered only the leptonic decay channel of the tau-lepton.

90% C.L. $\sqrt{s} = 3000$ GeV		
$\mathcal{L}(\text{fb}^{-1})$	$\lvert\tilde{\kappa}_{\nu_\tau}\rvert$ (10^{-7})	$\lvert\tilde{d}_{\nu_\tau}\rvert(10^{-18})(e$ cm$)$
100	7.826	15.160
500	5.234	10.140
1000	4.402	8.530
2000	3.702	7.174
3000	3.345	6.483
$\delta_{\text{sys}} = 5\%$	3.029×10^{-6}	5.871×10^{-17}
$\delta_{\text{sys}} = 10\%$	4.248×10^{-6}	8.233×10^{-17}
95% C.L. $\sqrt{s} = 3000$ GeV		
100	8.538	16.540
500	5.710	11.060
1000	4.802	9.306
2000	4.038	7.826
3000	3.649	7.072
$\delta_{\text{sys}} = 5\%$	3.268×10^{-6}	6.333×10^{-17}
$\delta_{\text{sys}} = 10\%$	4.622×10^{-6}	8.957×10^{-17}

TABLE XIII. Limits on the $\tilde{\kappa}_{\nu_\tau}$ magnetic moment and $\tilde{d}_{\nu_\tau}$ electric dipole moment via the process $\gamma e^- \to \tau\bar{\nu}_\tau\nu_e$ (γ is the Compton backscattering photon) for $P_{e^-} = -80\%$, and we considered only the leptonic decay channel of the tau-lepton.

90% C.L. $\sqrt{s} = 3000$ GeV		
$\mathcal{L}(\text{fb}^{-1})$	$\lvert\tilde{\kappa}_{\nu_\tau}\rvert$ (10^{-7})	$\lvert\tilde{d}_{\nu_\tau}\rvert(10^{-18})(e$ cm$)$
100	6.762	13.100
500	4.522	8.762
1000	3.802	7.368
2000	3.197	6.196
3000	2.889	5.598
$\delta_{\text{sys}} = 5\%$	3.029×10^{-6}	5.851×10^{-17}
$\delta_{\text{sys}} = 10\%$	4.248×10^{-6}	8.236×10^{-17}
95% C.L. $\sqrt{s} = 3000$ GeV		
100	7.377	14.290
500	4.933	9.560
1000	4.148	8.039
2000	3.488	6.760
3000	3.152	6.108
$\delta_{\text{sys}} = 5\%$	3.273×10^{-6}	6.343×10^{-17}
$\delta_{\text{sys}} = 10\%$	4.629×10^{-6}	8.971×10^{-17}

TABLE XIV. Limits on the $\tilde{\kappa}_{\nu_\tau}$ magnetic moment and $\tilde{d}_{\nu_\tau}$ electric dipole moment via the process $\gamma e^- \to \tau\bar{\nu}_\tau\nu_e$ (γ is the Compton backscattering photon) for $P_{e^-} = 0\%$, and we considered only the hadronic decay channel of the tau-lepton.

90% C.L. $\sqrt{s} = 1500$ GeV		
$\mathcal{L}(\text{fb}^{-1})$	$\lvert\tilde{\kappa}_{\nu_\tau}\rvert$ (10^{-7})	$\lvert\tilde{d}_{\nu_\tau}\rvert(10^{-17})(e$ cm)
100	14.400	2.791
200	12.110	2.347
500	9.632	1.866
1000	8.098	1.569
1500	7.319	1.418
$\delta_{\text{sys}} = 5\%$	6.869×10^{-6}	1.329×10^{-16}
$\delta_{\text{sys}} = 10\%$	9.701×10^{-6}	1.879×10^{-16}
95% C.L. $\sqrt{s} = 1500$ GeV		
100	15.710	3.045
200	13.210	2.560
500	10.500	2.036
1000	8.837	1.712
1500	7.985	1.547
$\delta_{\text{sys}} = 5\%$	7.484×10^{-6}	1.450×10^{-16}
$\delta_{\text{sys}} = 10\%$	10.580×10^{-6}	2.051×10^{-16}

TABLE XVI. Limits on the $\tilde{\kappa}_{\nu_\tau}$ magnetic moment and $\tilde{d}_{\nu_\tau}$ electric dipole moment via the process $\gamma e^- \to \tau\bar{\nu}_\tau\nu_e$ (γ is the Compton backscattering photon) for $P_{e^-} = -80\%$, and we considered only the hadronic decay channel of the tau-lepton.

90% C.L. $\sqrt{s} = 1500$ GeV		
Luminosity (fb^{-1})	$\lvert\tilde{\kappa}_{\nu_\tau}\rvert$ (10^{-7})	$\lvert\tilde{d}_{\nu_\tau}\rvert(10^{-17})(e$ cm)
100	12.440	2.411
200	10.460	2.027
500	8.320	1.612
1000	6.996	1.355
1500	6.322	1.225
$\delta_{\text{sys}} = 5\%$	6.865×10^{-6}	1.330×10^{-16}
$\delta_{\text{sys}} = 10\%$	9.709×10^{-6}	1.881×10^{-16}
95% C.L. $\sqrt{s} = 1500$ GeV		
100	13.570	2.630
200	11.410	2.212
500	9.078	1.759
1000	7.633	1.479
1500	6.897	1.336
$\delta_{\text{sys}} = 5\%$	7.490×10^{-6}	1.451×10^{-16}
$\delta_{\text{sys}} = 10\%$	10.590×10^{-6}	2.052×10^{-16}

In both cases the obtained sensitivity are for the values of $\sqrt{s} = 3000$ GeV, $\mathcal{L} = 3000$ fb^{-1} and 95% C.L. Comparing both cases, unpolarized and polarized electron beam, we conclude that the case with polarized beam $P_{e^-} = -80\%$ improves the sensitivity on the anomalous dipole moments in 13.63% with respect to the unpolarized case.

When only the hadronic decay channel of the tau-lepton is considered, the sensibility on the dipole moments is $|\tilde{\kappa}_{\nu_\tau}| = 3.127 \times 10^{-7}$, $|\tilde{d}_{\nu_\tau}(e\text{ cm})| = 6.059 \times 10^{-18}$ with

TABLE XV. Limits on the $\tilde{\kappa}_{\nu_\tau}$ magnetic moment and $\tilde{d}_{\nu_\tau}$ electric dipole moment via the process $\gamma e^- \to \tau\bar{\nu}_\tau\nu_e$ (γ is the Compton backscattering photon) for $P_{e^-} = 0\%$, and we considered only the hadronic decay channel of the tau-lepton.

90% C.L. $\sqrt{s} = 3000$ GeV		
$\mathcal{L}(\text{fb}^{-1})$	$\lvert\tilde{\kappa}_{\nu_\tau}\rvert$ (10^{-7})	$\lvert\tilde{d}_{\nu_\tau}\rvert(10^{-18})(e$ cm)
100	6.704	12.990
500	4.484	8.689
1000	3.771	7.308
2000	3.171	6.146
3000	2.866	5.554
$\delta_{\text{sys}} = 5\%$	2.995×10^{-6}	5.805×10^{-17}
$\delta_{\text{sys}} = 10\%$	4.236×10^{-6}	8.209×10^{-17}
95% C.L. $\sqrt{s} = 3000$ GeV		
100	7.314	14.170
500	4.892	9.480
1000	4.114	7.972
2000	3.460	6.705
3000	3.127	6.059
$\delta_{\text{sys}} = 5\%$	3.268×10^{-6}	6.333×10^{-17}
$\delta_{\text{sys}} = 10\%$	4.622×10^{-6}	8.956×10^{-17}

TABLE XVII. Limits on the $\tilde{\kappa}_{\nu_\tau}$ magnetic moment and $\tilde{d}_{\nu_\tau}$ electric dipole moment via the process $\gamma e^- \to \tau\bar{\nu}_\tau\nu_e$ (γ is the Compton backscattering photon) for $P_{e^-} = -80\%$, and we considered only the hadronic decay channel of the tau-lepton.

90% C.L. $\sqrt{s} = 3000$ GeV		
Luminosity (fb^{-1})	$\lvert\tilde{\kappa}_{\nu_\tau}\rvert$ (10^{-7})	$\lvert\tilde{d}_{\nu_\tau}\rvert(10^{-18})(e$ cm)
100	5.792	11.22
500	3.873	7.506
1000	3.257	6.312
2000	2.739	5.307
3000	2.475	4.976
$\delta_{\text{sys}} = 5\%$	3.000×10^{-6}	5.814×10^{-17}
$\delta_{\text{sys}} = 10\%$	4.243×10^{-6}	8.222×10^{-17}
95% C.L. $\sqrt{s} = 3000$ GeV		
100	6.319	12.240
500	4.226	8.189
1000	3.553	6.886
2000	2.988	5.791
3000	2.700	5.232
$\delta_{\text{sys}} = 5\%$	3.273×10^{-6}	6.343×10^{-17}
$\delta_{\text{sys}} = 10\%$	4.629×10^{-6}	8.971×10^{-17}

$P_{e^-}=0\%$ and $|\tilde{\kappa}_{\nu_\tau}|=2.700\times10^{-7}$, $|\tilde{d}_{\nu_\tau}(e\ \mathrm{cm})|=5.232\times10^{-18}$ with $P_{e^-}=-80\%$, respectively. The obtained results are with $\sqrt{s}=3000$ GeV, $\mathcal{L}=3000\ \mathrm{fb}^{-1}$ and 95% C.L. The comparison of both cases shows that the case with polarized electron beam improves the sensitivity of the anomalous dipole moments of the τ-neutrino of 13.65%, with respect to the case with $P_{e^-}=0\%$.

If now we compare the cases with leptonic decay channel and hadronic decay channel with $P_{e^-}=0\%$ and $\sqrt{s}=3000$ GeV, $\mathcal{L}=3000\ \mathrm{fb}^{-1}$ and 95% C.L. the improvement in sensitivity is 14.31% for the hadronic decay channel with respect to the leptonic decay channel, whereas for $P_{e^-}=-80\%$ the improvement in the sensitivity is of 14.34% with respect to the case of the leptonic decay channel. These differences are expected for the different cases because the tau-lepton decays roughly 35% of the time leptonically and 65% of the time hadronically.

K. 90% C.L and 95% C.L bounds on the anomalous ν_τMM and ν_τEDM with unpolarized and polarized electron beams, including ISR + BS effects

Our results on the $\tilde{\kappa}_{\nu_\tau}$ and $\tilde{d}_{\nu_\tau}(e\ \mathrm{cm})$ through the process $\gamma e^-\to\tau\bar{\nu}_\tau\nu_e$ and considering the background coming from ISR and BS are presented in Tables XVIII and XIX, for the unpolarized and polarized cases. We consider the leptonic (hadronic) decay channel of the tau-lepton, $P_{e^-}=0\%(-80\%)$ and $\sqrt{s}=3000$ GeV.

TABLE XVIII. Limits on the $\tilde{\kappa}_{\nu_\tau}$ magnetic moment and $\tilde{d}_{\nu_\tau}$ electric dipole moment via the process $\gamma e^-\to\tau\bar{\nu}_\tau\nu_e$ (γ is the Compton backscattering photon) for $P_{e^-}=0\%$, and we considered only the leptonic decay channel of the tau-lepton. We include ISR + BS effects.

90% C.L. $\sqrt{s}=3000$ GeV		
$\mathcal{L}(\mathrm{fb}^{-1})$	$\lvert\tilde{\kappa}_{\nu_\tau}\rvert$ (10^{-7})	$\lvert\tilde{d}_{\nu_\tau}\rvert(10^{-18})(e\ \mathrm{cm})$
100	8.590	16.646
500	5.744	11.132
1000	4.830	9.361
2000	4.062	7.871
3000	3.670	7.113
$\delta_{\mathrm{sys}}=5\%$	3.273×10^{-6}	6.342×10^{-17}
$\delta_{\mathrm{sys}}=10\%$	4.628×10^{-6}	8.969×10^{-17}
95% C.L. $\sqrt{s}=3000$ GeV		
100	9.372	18.162
500	6.267	12.146
1000	5.270	10.213
2000	4.432	8.588
3000	4.004	7.760
$\delta_{\mathrm{sys}}=5\%$	3.571×10^{-6}	6.920×10^{-17}
$\delta_{\mathrm{sys}}=10\%$	5.050×10^{-6}	9.786×10^{-17}

TABLE XIX. Limits on the $\tilde{\kappa}_{\nu_\tau}$ magnetic moment and $\tilde{d}_{\nu_\tau}$ electric dipole moment via the process $\gamma e^-\to\tau\bar{\nu}_\tau\nu_e$ (γ is the Compton backscattering photon) for $P_{e^-}=-80\%$, and we considered only the hadronic decay channel of the tau-lepton. We include ISR + BS effects.

90% C.L. $\sqrt{s}=3000$ GeV		
Luminosity (fb^{-1})	$\lvert\tilde{\kappa}_{\nu_\tau}\rvert$ (10^{-7})	$\lvert\tilde{d}_{\nu_\tau}\rvert(10^{-18})(e\ \mathrm{cm})$
100	7.414	14.368
500	4.958	9.608
1000	4.169	8.079
2000	3.506	6.794
3000	3.168	6.139
$\delta_{\mathrm{sys}}=5\%$	3.270×10^{-6}	6.342×10^{-17}
$\delta_{\mathrm{sys}}=10\%$	4.625×10^{-6}	8.969×10^{-17}
95% C.L. $\sqrt{s}=3000$ GeV		
100	8.089	15.676
500	5.409	10.483
1000	4.549	8.815
2000	3.825	7.412
3000	3.456	6.698
$\delta_{\mathrm{sys}}=5\%$	3.568×10^{-6}	6.920×10^{-17}
$\delta_{\mathrm{sys}}=10\%$	5.046×10^{-6}	9.786×10^{-17}

It is seen of the comparison from Tables XI and XVIII that ISR and BS effects lead to decreasing the sensitivity on the $\tilde{\kappa}_{\nu_\tau}$ and $\tilde{d}_{\nu_\tau}(e\ \mathrm{cm})$. This decrease is of the order 8.85%. In the case of Tables XVII and XIX, it is of the order 20.4% of difference in sensitivity for $\tilde{\kappa}_{\nu_\tau}$ and $\tilde{d}_{\nu_\tau}(e\ \mathrm{cm})$. It is seen that ISR plus BS effects are more effective for the polarized case than for the unpolarized case.

III. CONCLUSIONS

In this paper, we have sensitivity estimates on the total cross section and on the dipole moments $\tilde{\kappa}_{\nu_\tau}$ and $\tilde{d}_{\nu_\tau}$ through the process $e^+e^-\to\nu_\tau\bar{\nu}_\tau\gamma$ at the future CLIC. Furthermore, the process is analyzed for four scenarios motivated by the strong advantage in searching for new physics BSM: (a) unpolarized electron-positron beam $(P_{e^-},P_{e^+})=(0\%,0\%)$, (b) polarized electron-positron beam $(P_{e^-},P_{e^+})=(-80\%,60\%)$, (c) unpolarized electron-positron beam $(P_{e^-},P_{e^+})=(0\%,0\%)$, including ISR + BS effects, and (d) polarized electron-positron beam $(P_{e^-},P_{e^+})=(-80\%,60\%)$, with ISR + BS effects. In the first scenario, the unpolarized cross section has the value of ≈200(200) pb (see Figs. 2 and 3) depending on the anomalous coupling type $\tilde{\kappa}_{\nu_\tau}(\tilde{d}_{\nu_\tau})$. In the second scenario, which is motivated by the possibility to enhance or suppress different physical processes, the polarized cross section gets a value of ≈300(300) pb (see Figs. 7 and 8) depending on the anomalous coupling type $\tilde{\kappa}_{\nu_\tau}(\tilde{d}_{\nu_\tau})$. For the third and fourth scenarios, the incorporation of the

backgrounds coming from ISR + BS has the effect of decreasing the sensitivity bounds on $\tilde{\kappa}_{\nu_\tau}$ and $\tilde{d}_{\nu_\tau}$ as shown in Tables VIII and IX. Comparing the (a) and (b) scenarios shows that the cross section is enhanced for 100 pb for the case of the polarized electron-positron beam. The option of upgrading the incoming electron and the positron beam to be polarized has the power to enhance the potential of the machine. In addition to these, the results for the sensitivity contours in the $\tilde{\kappa}_{\nu_\tau} - \tilde{d}_{\nu_\tau}$ plane for the unpolarized and polarized case are presented (see Figs. 4–6 and 9–11).

Figures 2–11 and Tables I–VI and VIII and IX highlight that sensitivity estimates for the total cross section, as well as for the anomalous $\tilde{\kappa}_{\nu_\tau}$ and $\tilde{d}_{\nu_\tau}$ at CLIC for high center-of-mass energies and high luminosities, reach a better sensitivity to that of L3 [20], CERN-WA-066 [19] and E872 (DONUT) [18], as well as of others experimental and theoretical results (see Table I of Ref. [16]). The most optimistic scenario about the sensitivity in the anomalous dipole moments of the τ-neutrino (see Tables III and VI), yields the following results: $|\tilde{\kappa}_{\nu_\tau}| = 2.103 \times 10^{-7}$ and $|\tilde{d}_{\nu_\tau}(e\,\mathrm{cm})| = 4.076 \times 10^{-18}$ with $(P_{e^-}, P_{e^+}) = (0\%, 0\%)$. In addition, we also obtain the results $|\tilde{\kappa}_{\nu_\tau}| = 2.002 \times 10^{-7}$ and $|\tilde{d}_{\nu_\tau}(e\ \mathrm{cm})| = 4.039 \times 10^{-18}$ with $(P_{e^-}, P_{e^+}) = (-80\%, 60\%)$. Our results show the potential and the feasibility of the process $e^+e^- \to \nu_\tau \bar{\nu}_\tau \gamma$ at the CLIC.

In the case of the process $\gamma e^- \to \tau \bar{\nu}_\tau \nu_e$, we have studied the ν_τMM and ν_τEDM in a model-independent way. For the four options that we considered in this paper: polarized electron beam, unpolarized electron beam, polarized electron beam with ISR + BS effects and unpolarized electron beam including ISR + BS effects, our results are sensitive to the parameters of the collider such as the center-of-mass energy and the luminosity. Furthermore, our results are also sensitive to the kinematic basic acceptance cuts of the final state particles p_T^ν, η^τ and p_T^τ, as well as the systematic uncertainties δ_{sys}. A good knowledge of the kinematic cuts is needed not only to improve sensitivity analyses, but because it can help to understand which are the most appropriate processes to probing in the future high-energy and high-luminosity linear colliders, such as the CLIC. CLIC, as well as any γe^- Compton backscattering experiment, offers a good laboratory to study the total cross section and the dipole moments of the tau-neutrino through the process $\gamma e^- \to \tau \bar{\nu}_\tau \nu_e$ with unpolarized and polarized electron beam.

Despite the large number of studies performed in recent years on the electromagnetic properties of the tau-neutrino, more studies are still needed to deeply understand and explain experimental observations and their comparison with model predictions. Current and future data of the ATLAS [78] and CMS [79,80] collaborations, as well as new analysis of already existing data sets, could help to improve our knowledge on the ν_τMM and ν_τEDM [16].

A precision machine like CLIC is expected to help in the precise estimates of the anomalous coupling $\nu_\tau \bar{\nu}_\tau \gamma$. The reach of the CLIC with maximum $\sqrt{s} = 3000$ GeV and $\mathcal{L} = 3000\ \mathrm{fb}^{-1}$ to probing the relevant observable of the process is presented. The influence of the anomalous couplings, of the kinematic cuts, of the uncertainties systematic, as well as the polarized electron beam on the cross section, the tau-lepton pseudorapidity distribution and the tau-lepton transverse momentum distribution are studied. Furthermore, we estimate the sensitivity on the anomalous ν_τMM and ν_τEDM. Our results are summarized in Figs. 13–26 as well as in Tables X–XIX, respectively.

From our set of figures and tables it is evident that a suitably chosen beam polarization is found to be advantageous as illustrated with an 80% left-polarization electron beam (see Figs. 21–26). The most optimistic scenario about the sensitivity in the anomalous dipole moments of the tau-neutrino (see Tables XIII and XVII) yields the following results: $|\tilde{\kappa}_{\nu_\tau}| = 2.889 \times 10^{-7}$ and $|\tilde{d}_{\nu_\tau}(e\ \mathrm{cm})| = 5.598 \times 10^{-18}$ with $P_{e^-} = -80\%$ and we considered only the leptonic decay channel of the tau-lepton. $|\tilde{\kappa}_{\nu_\tau}| = 2.475 \times 10^{-7}$ and $|\tilde{d}_{\nu_\tau}(e\ \mathrm{cm})| = 4.976 \times 10^{-18}$ with $P_{e^-} = -80\%$ and we take into account only the hadronic decay channel of the tau-lepton. Our results show the potential and the feasibility of the process $\gamma e^- \to \tau \bar{\nu}_\tau \nu_e$ at the CLIC at the γe^- mode.

The incorporation of the background coming from ISR + BS has the effect of decreasing the total cross section of the signal $e^+e^- \to \nu_\tau \bar{\nu}_\tau \gamma$ and $\gamma e^- \to \tau \bar{\nu}_\tau \nu_e$, as well as the sensitivity estimate on $\tilde{\kappa}_{\nu_\tau}$ and $\tilde{d}_{\nu_\tau}$. However, is essential have a precise knowledge if we wish to make any realistic predictions at the future linear colliders, such as the CLIC.

In conclusion, both processes $e^+e^- \to \nu_\tau \bar{\nu}_\tau \gamma$ and $\gamma e^- \to \tau \bar{\nu}_\tau \nu_e$ are very useful to sensitivity probing on the dipole moments of the tau-neutrino and illustrate the complementarity between CLIC and other e^+e^- and pp colliders for probing extensions of the SM. However, the process $e^+e^- \to \nu_\tau \bar{\nu}_\tau \gamma$ is more sensitive to model-independent sensibility study for the tau-neutrino electromagnetic dipole moments at the CLIC with polarized electron-positron beams.

ACKNOWLEDGMENTS

A. G. R. and M. A. H. R acknowledge support from Sistena Nacional de Investigadores (SNI) and Programa de Fortalecimiento de la Calidad en Instituciones Educativas (PROFOCIE, México).

[1] S. L. Glashow, Nucl. Phys. **22**, 579 (1961).
[2] S. Weinberg, Phys. Rev. Lett. **19**, 1264 (1967).
[3] A. Salam, in *Elementary Particle Theory*, edited by N. Svartholm (Almquist and Wiskell, Stockholm, 1968), p. 367.
[4] K. Fujikawa and R. Shrock, Phys. Rev. Lett. **45**, 963 (1980).
[5] R. E. Shrock, Nucl. Phys. **B206**, 359 (1982).
[6] M. Fukugita and T. Yanagida, *Physics of Neutrinos and Applications to Astrophysics* (Springer, Berlin, 2003).
[7] A. Cisneros, Astrophys. Space Sci. **10**, 87 (1971).
[8] M. Zralek, Acta Phys. Pol. B **28**, 2225 (1997).
[9] A. D. Sakharov, Pis'ma Zh. Eksp. Teor. Fiz. **5**, 32 (1967); JETP Lett. **5**, 24 (1967); Sov. Phys. Usp. **34**, 392 (1991); Usp. Fiz. Nauk **161**, 61 (1991).
[10] J. H. Christenson, J. W. Cronin, V. L. Fitch, and R. Turlay, Phys. Rev. Lett. **13**, 138 (1964).
[11] K. Abe *et al.*, Phys. Rev. Lett. **87**, 091802 (2001).
[12] R. Aaij *et al.* (LHCb Collaboration), J. High Energy Phys. 07 (2014) 041.
[13] A. G. Bed, V. B. Brudanin, V. G. Egorov, D. V. Medvedev, V. S. Pogosov, M. V. Shirchenko, and A. S. Starostin (GEMMA Collaboration), Adv. High Energy Phys. **2012**, 350150 (2012).
[14] L. B. Auerbach *et al.* (LSND Collaboration), Phys. Rev. D **63**, 112001 (2001).
[15] F. del Aguila and M. Sher, Phys. Lett. B **252**, 116 (1990).
[16] A. Gutiérrez-Rodríguez, M. Koksal, A. A. Billur, and M. A. Hernández-Ruíz, arXiv:1712.02439.
[17] C. Arpesella *et al.* (Borexino Collaboration), Phys. Rev. Lett. **101**, 091302 (2008).
[18] R. Schwinhorst *et al.* (DONUT Collaboration), Phys. Lett. B **513**, 23 (2001).
[19] A. M. Cooper-Sarkar, S. Sarkar, J. Guy, W. Venus, P. O. Hulth, and K. Hultqvist (WA66 Collaboration), Phys. Lett. B **280**, 153 (1992).
[20] M. Acciarri *et al.* (L3 Collaboration), Phys. Lett. B **412**, 201 (1997).
[21] A. Llamas-Bugarin, A. Gutiérrez-Rodríguez, and M. A. Hernández-Ruíz, Phys. Rev. D **95**, 116008 (2017).
[22] A. Gutiérrez-Rodríguez, M. Koksal, and A. A. Billur, Phys. Rev. D **91**, 093008 (2015).
[23] A. Gutiérrez-Rodríguez, M. Koksal, and A. A. Billur, Proc. Sci. EPS-HEP2015 (**2015**) 036.
[24] A. Gutiérrez-Rodríguez, Int. J. Theor. Phys. **54**, 236 (2015).
[25] A. Gutiérrez-Rodríguez, Adv. High Energy Phys. **2014**, 491252 (2014).
[26] C. Patrignani *et al.* (Particle Data Group), Chin. Phys. C **40**, 100001 (2016).
[27] A. Gutiérrez-Rodríguez, Pramana J. Phys. **79**, 903 (2012).
[28] A. Gutiérrez-Rodríguez, Eur. Phys. J. C **71**, 1819 (2011).
[29] C. Aydin, M. Bayar, and N. Kilic, Chin. Phys. C **32**, 608 (2008).
[30] A. Gutiérrez-Rodríguez, M. A. Hernández-Ruíz, B. Jayme-Valdés, and M. A. Pérez, Phys. Rev. D **74**, 053002 (2006).
[31] A. Gutiérrez-Rodríguez, M. A. Hernández-Ruíz, and A. Del Rio-De Santiago, Phys. Rev. D **69**, 073008 (2004).
[32] A. Gutiérrez-Rodríguez and M. A. Hern´andez-Ru´ız, Acta Phys. Slovaca **53**, 293 (2003).
[33] K. Akama, T. Hattori, and K. Katsuura, Phys. Rev. Lett. **88**, 201601 (2002).
[34] A. Aydemir and R. Sever, Mod. Phys. Lett. A **16**, 457 (2001).
[35] A. Gutiérrez-Rodríguez, M. A. Hernández, A. Rosado, and M. Maya, Rev. Mex. Fís. **45**, 249 (1999).
[36] A. Gutiérrez, M. A. Hernández, M. Maya, and A. Rosado, Phys. Rev. D **58**, 117302 (1998).
[37] P. Abreu *et al.* (DELPHI Collaboration), Z. Phys. C **74**, 577 (1997).
[38] R. Escribano and E. Massó, Phys. Lett. B **395**, 369 (1997).
[39] T. M. Gould and I. Z. Rothstein, Phys. Lett. B **333**, 545 (1994).
[40] H. Grotch and R. Robinet, Z. Phys. C **39**, 553 (1988).
[41] I. Sahin, Phys. Rev. D **85**, 033002 (2012).
[42] I. Sahin and M. Koksal, J. High Energy Phys. 03 (2011) 100.
[43] E. Accomando *et al.* (CLIC Physics Working Group), arXiv: hep-ph/0412251.
[44] D. Dannheim, P. Lebrun, L. Linssen *et al.*, arXiv:1208.1402.
[45] H. Abramowicz *et al.* (CLIC Detector and Physics Study Collaboration), arXiv:1307.5288.
[46] J. F. Nieves, Phys. Rev. D **26**, 3152 (1982).
[47] B. Kayser and A. Goldhaber, Phys. Rev. D **28**, 2341 (1983).
[48] B. Kayser, Phys. Rev. D **30**, 1023 (1984).
[49] P. Vogel and J. Engel, Phys. Rev. D **39**, 3378 (1989).
[50] J. Bernabeu, L. Cabral-Rosetti, J. Papavassiliou, and J. Vidal, Phys. Rev. D **62**, 113012 (2000).
[51] J. Bernabéu, J. Papavassiliou, and J. Vidal, Phys. Rev. Lett. **89**, 101802 (2002); **89**, 229902(E) (2002).
[52] M. S. Dvornikov and A. I. Studenikin, J. Exp. Theor. Phys. **99**, 254 (2004).
[53] C. Giunti and A. Studenikin, Phys. At. Nucl. **72**, 2089 (2009).
[54] C. Broggini, C. Giunti, and A. Studenikin, Adv. High Energy Phys. **2012**, 1 (2012).
[55] R. Escribano and E. Massó, Nucl. Phys. **B429**, 19 (1994).
[56] W. Buchmuller and D. Wyler, Nucl. Phys. **B268**, 621 (1986).
[57] C. N. Leung, S. T. Love, and S. Rao, Z. Phys. C **31**, 433 (1986).
[58] A. Belyaev, N. D. Christensen, and A. Pukhov, Comput. Phys. Commun. **184**, 1729 (2013).
[59] M. Köksal, A. A. Billur, and A. Gutiérrez-Rodríguez, Adv. High Energy Phys. **2017**, 6738409 (2017).
[60] Y. Özgüven, S. C. Inan, A. A. Billur, M. Köksal, and M. K. Bahar, Nucl. Phys. **B923**, 475 (2017).
[61] M. Köksal, S. C. Inan, A. A. Billur, Y. Özgüven, and M. K. Bahar, Phys. Lett. B **783**, 375 (2018).
[62] M. Köksal, A. A. Billur, A. Gutiérrez-Rodríguez, and M. A. Hernández-Ruíz, Phys. Rev. D **98**, 015017 (2018).
[63] A. A. Billur, M. Köksal, and A. Gutiérrez-Rodríguez, Phys. Rev. D **96**, 056007 (2017).
[64] A. A. Billur and M. Köksal, Phys. Rev. D **89**, 037301 (2014).
[65] G. Moortgat-Pick *et al.*, Phys. Rep. **460**, 131 (2008).
[66] P. Chen, Differential luminosity under multiphoton beamstrahlung, SLAC Report No. SLAC-PUB-5615 (1991).
[67] P. Chen, Phys. Rev. D **46**, 1186 (1992).
[68] J. Brau *et al.*, International Linear Collider Reference Design Report Vol. 3: Accelerator, Report No. ILC-REPORT-2007-001 (2007).

[69] H. Braun *et al.*, CLIC 2008 Parameters, CERN Reports No. CERN-OPEN-2008-21 and No. CLIC-NOTE-764, Geneva (2008).
[70] I. F. Ginzburg, G. L. Kotkin, V. G. Serbo, and V. I. Telnov, Nucl. Instrum. Methods Phys. Res. **205**, 47 (1983).
[71] V. M. Arutyunyan, F. R. Arutyunyan, K. A. Ispiryan, and V. A. Tumanyan, Sov. Phys. JETP **18**, 873 (1964).
[72] R. H. Milburn, Phys. Rev. Lett. **10**, 75 (1963).
[73] F. R. Arutyunyan and V. A. Tumanyan, Sov. Phys. JETP **17**, 1412 (1963).
[74] T. H. Tran, V. Balagura, V. Boudry, J. C. Brient, and H. Videau, Eur. Phys. J. C **76**, 468 (2016).
[75] M. Aicheler *et al.*, A multi-TeV linear collider based on CLIC technology: CLIC Conceptual Design Report, JAI-2012-001, KEK Report Nos. 2012-1, PSI-12-01, SLAC-R-985, https://edms.cern.ch/document/1234244/.
[76] L. Linssen *et al.*, Physics and detectors at CLIC: CLIC Conceptual Design Report, 2012, ANL-HEP-TR-12-01, CERN-2012-003, DESY 12-008, KEK Report No. 2011-7, arXiv:1202.5940.
[77] V. Ari, A. A. Billur, S. C. Inan, and M. Koksal, Nucl. Phys. **B906**, 211 (2016).
[78] G. Aad *et al.* (ATLAS Collaboration), Phys. Rev. D **93**, 112002 (2016).
[79] V. Khachatryan *et al.* (CMS Collaboration), Phys. Lett. B **760**, 448 (2016).
[80] V. Khachatryan *et al.* (CMS Collaboration), J. High Energy Phys. 04 (2015) 164.